



Polymeric complexes – LXI. Supramolecular structure, thermal properties, SS-DNA binding activity and antimicrobial activities of polymeric complexes of rhodanine hydrazone compounds



A.Z. El-Sonbati^a, M.A. Diab^a, A.A. El-Bindary^{a,*}, M.M. Ghoneim^b, M.T. Mohesien^c, M.K. Abd El-Kader^a

^a Chemistry Department, Faculty of Science, Damietta University, Damietta 34517, Egypt

^b Chemistry Department, Faculty of Science, Tanta University, Tanta, Egypt

^c Botany Department, Faculty of Science, Damietta University, Damietta 34517, Egypt

ARTICLE INFO

Article history:

Received 21 October 2015

Received in revised form 8 November 2015

Accepted 2 December 2015

Available online xxxx

Keywords:

Co(II) complexes

SS-DNA binding

Molecular structure

Antimicrobial activities

ABSTRACT

A series of new ligands 5-(4'-alkylphenylazo)-3-phenylamino-2-thioxothiazolidin-4-one (**HL_n**) were synthesized from the coupling of 3-phenylamino-2-thioxothiazolidin-4-one with aniline and its *p*-derivatives. These ligands and their Co(II) polymeric complexes of the [(Co)₂(L_n)₂(HL_n)(CH₃COO)₂(H₂O)₂]_n have been deduced from elemental analyses, IR, ¹H-NMR, X-ray diffraction and mass spectra as well as magnetic and thermal measurements. IR and ¹H NMR studies reveal that the ligands (**HL_n**) exist in the tautomeric enol/hydrazone form in both states with intramolecular hydrogen bonding. The important infrared (IR) spectral bands imply that **HL_n** is coordinated to the metal ion in a monobasic tetradentate *via* NH (hydrazone), oxygen of the carbonyl group (CO), nitrogen of the NH (3-phenylamine) and thion sulfur (CS) group. The complexes are polymeric, non-electrolytes, paramagnetic and octahedral six-coordinated. The molecular and electronic structures of the investigated compounds (**HL_n**) were also studied using quantum chemical calculations. The salmon sperm DNA (SS-DNA) binding activity of the ligands (**HL_n**) was studied by absorption spectra. The interaction between ligands (**HL_n**) and SS-DNA shows hypochromism effect coupled with obvious bathochromism. The values of binding constant are correlated with Hammett's constant (σ^R). The cytotoxic activity of ligands (**HL_n**) and their Co(II) complexes were tested against two human cancer HePG-2 (Hepatocellular carcinoma) and MCF-7 (breast cancer). The antioxidant activities of ligands (**HL_n**) and their Co(II) complexes were performed by ABTS method. The antimicrobial activity of ligands **HL_n** and their Co(II) complexes were tested against Gram negative bacteria (*Escherichia coli*), Gram positive bacteria (*Staphylococcus aureus*) and yeast (*Candida albicans*).

© 2015 Elsevier B.V. All rights reserved.

1. Introduction

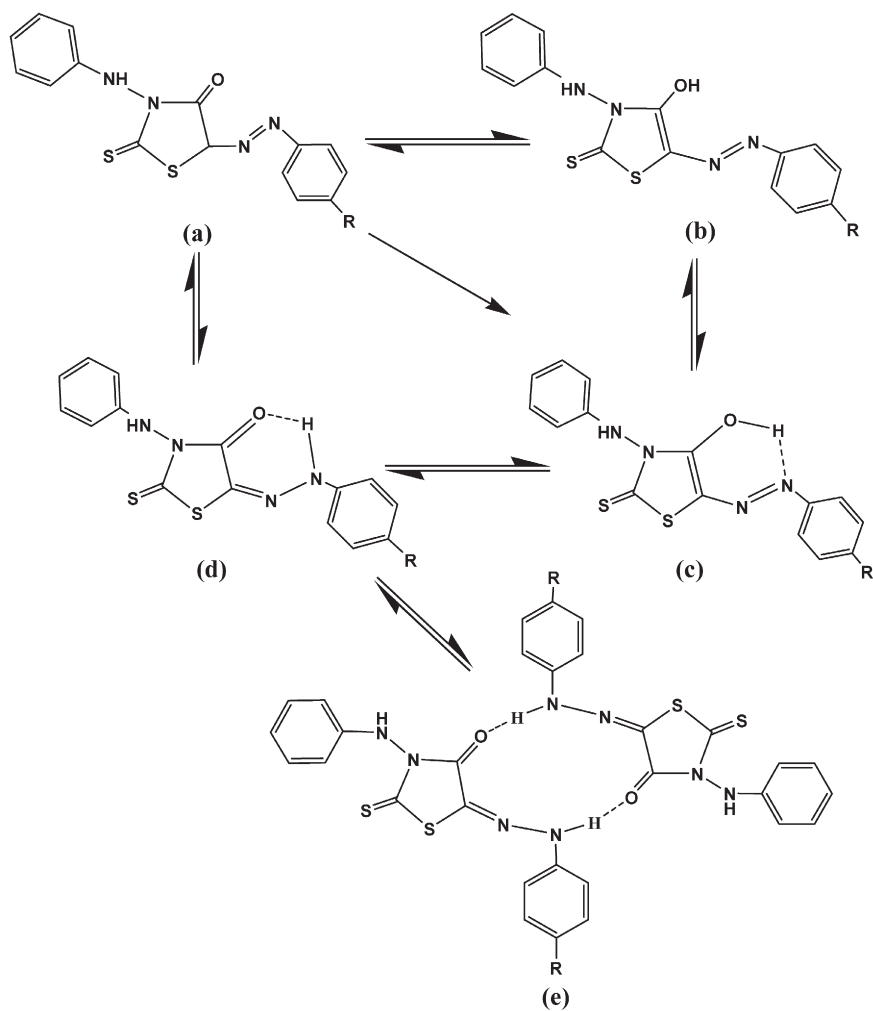
In recent past, a variety of molecules based on rhodanine have been synthesized and evaluated with improved pharmacological activities due to their wide range of pharmacological and clinical utilization [1–8]. Rhodanine compounds and their complexes play an important role in biological reactions [9,10]. These molecules are considered as good antimycobacterial, antifungal, antidiabetic, antihepatitis C virus (HCV), anticancer, antioxidant, pesticidal, antihypertensive and antineoplastic agents. These molecules attracted much attention and encouraged the chemists and biologists to extensive investigations or molecular manipulations [5,11]. Chemical properties of rhodanine and its derivatives are of interest due to coordination capacity and their use as metal extracting agents; these molecules are capable of having

keto–enol tautomers. Hydrazone compounds of rhodanine usually react as chelating with transition metal ions by bonding through the oxygen and hydrazinic nitrogen atoms [1,8], as they form a stable six-membered characterization of 5-(4'-alkylphenylazo)-3-phenylamino-2-thioxothiazolidin-4-one (**HL_n**) and their polymer complexes with cobalt(II). **HL_n** act as monobasic tetradentate reacting with Co(II) through the CO (rhodanine moiety), hydrazinic N with displacement of hydrogen atom, CS (rhodanine moiety) and amidic N.

DNA is one of the most important biomacromolecules in life processes because it carries inheritance information and instructs the biological synthesis of proteins and enzyme through the process of replication and transcription of genetic information. DNA plays an important role in the process of storing, copying and transmitting gene messages. DNA is also a major target for drugs and some harmful chemicals, and the studies on the binding nature of these small molecules to DNA are important and fundamental issues on life science because these drugs and chemicals can significantly influence the genetic information expression and result in some diseases

* Corresponding author.

E-mail address: abindary@yahoo.com (A.A. El-Bindary).



R = -OCH₃ (HL₁), -CH₃ (HL₂), -H (HL₃), -Cl (HL₄) and -NO₂ (HL₅)

Fig. 1. Structure of ligands (HL_n).

Table 1
Physical properties and elemental analyses data of the ligands (HL_n) and their Co(II) complexes (1–5).

Compound	M.P. (°C)	% Exp. (calc.)				Composition
		C	H	N	M	
HL ₁	131	53.60 (53.63)	4.00 (3.91)	15.60 (15.64)	–	[(Co) ₂ (HL ₁)(L ₁) ₂ (CH ₃ COO) ₂ (H ₂ O) ₂] _n
(1)	–	46.22 (46.43)	3.56 (3.72)	12.12 (12.50)	8.37 (8.77)	
HL ₂	161	56.00 (56.14)	4.10 (4.09)	16.40 (16.37)	–	[(Co) ₂ (HL ₂)(L ₂) ₂ (CH ₃ COO) ₂ (H ₂ O) ₂] _n
(2)	–	48.03 (48.15)	3.66 (3.86)	12.74 (12.96)	8.78 (9.10)	
HL ₃	164	54.90 (54.88)	3.70 (3.66)	17.10 (17.07)	–	[(Co) ₂ (HL ₃)(L ₃) ₂ (CH ₃ COO) ₂ (H ₂ O) ₂] _n
(3)	–	46.77 (46.89)	3.35 (3.51)	12.04 (13.40)	(9.40)	
HL ₄	164	49.70 (49.66)	3.10 (3.03)	15.50 (15.45)	–	[(Co) ₂ (HL ₄)(L ₄) ₂ (CH ₃ COO) ₂ (H ₂ O) ₂] _n
(4)	–	43.14 (43.32)	2.89 (3.02)	12.03 (12.38)	8.47 (8.68)	
HL ₅	178	48.30 (48.26)	3.00 (2.95)	18.80 (18.77)	–	[(Co) ₂ (HL ₅)(L ₅) ₂ (CH ₃ COO) ₂ (H ₂ O) ₂] _n
(5)	–	42.12 (42.34)	2.87 (2.95)	14.86 (15.12)	8.15 (8.49)	

^aMicroanalytical data as well as metal estimations are in good agreement with the stoichiometry of the proposed complexes.

^bThe excellent agreement between calculated and experimental data supports the assignment suggested in the present work.

^cHL₁–HL₅ are the ligands and L₁–L₅ are the anions.

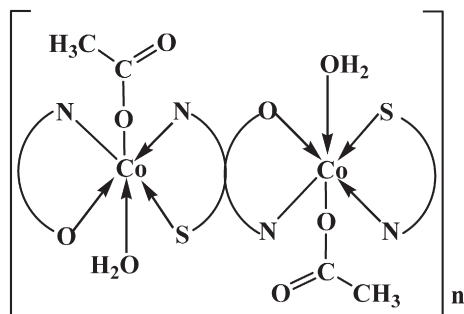


Fig. 2. Proposed structure of Co(II) complexes.

related to the cell proliferation and differentiation [12,13]. In our laboratories, we have initiated a series of studies of the effects of substituents at *p*-position of the aromatic amine on the stoichiometries of

the complexes of these ligands with cobalt acetate [7]. The Co(II) complexes attracted attention in coordination chemistry, thermal stability and biological function of some bimetallic complexes for which structural information was obtained by spectrochemical and magnetochemical means; due to the Co(II) in d^7 is known, in four coordinate as tetrahedral and six coordinate as octahedral stereochemistries [14–18].

The aim of this work is to, synthesis and characterize of Co(II) complexes of 5-(4'-alkylphenylazo)-3-phenylamino-2-thioxothiazolidin-4-one (HL_n) by elemental analyses, IR, 1H & ^{13}C NMR, UV-Vis, X-ray diffractometer, magnetic moment, molar conductance, and thermal analysis. Molecular and electronic structures of the ligands (HL_1 , HL_3 and HL_4) were discussed. Mass spectra and X-ray diffraction analysis of ligands (HL_1 , HL_3 and HL_4) were discussed. The activation thermodynamic parameters, such as activation energy (E_a), enthalpy (ΔH^*), entropy (ΔS^*), and Gibbs free energy change of the decomposition (ΔG^*) were calculated using Coats–Redfern and Horowitz–Metzger methods. The

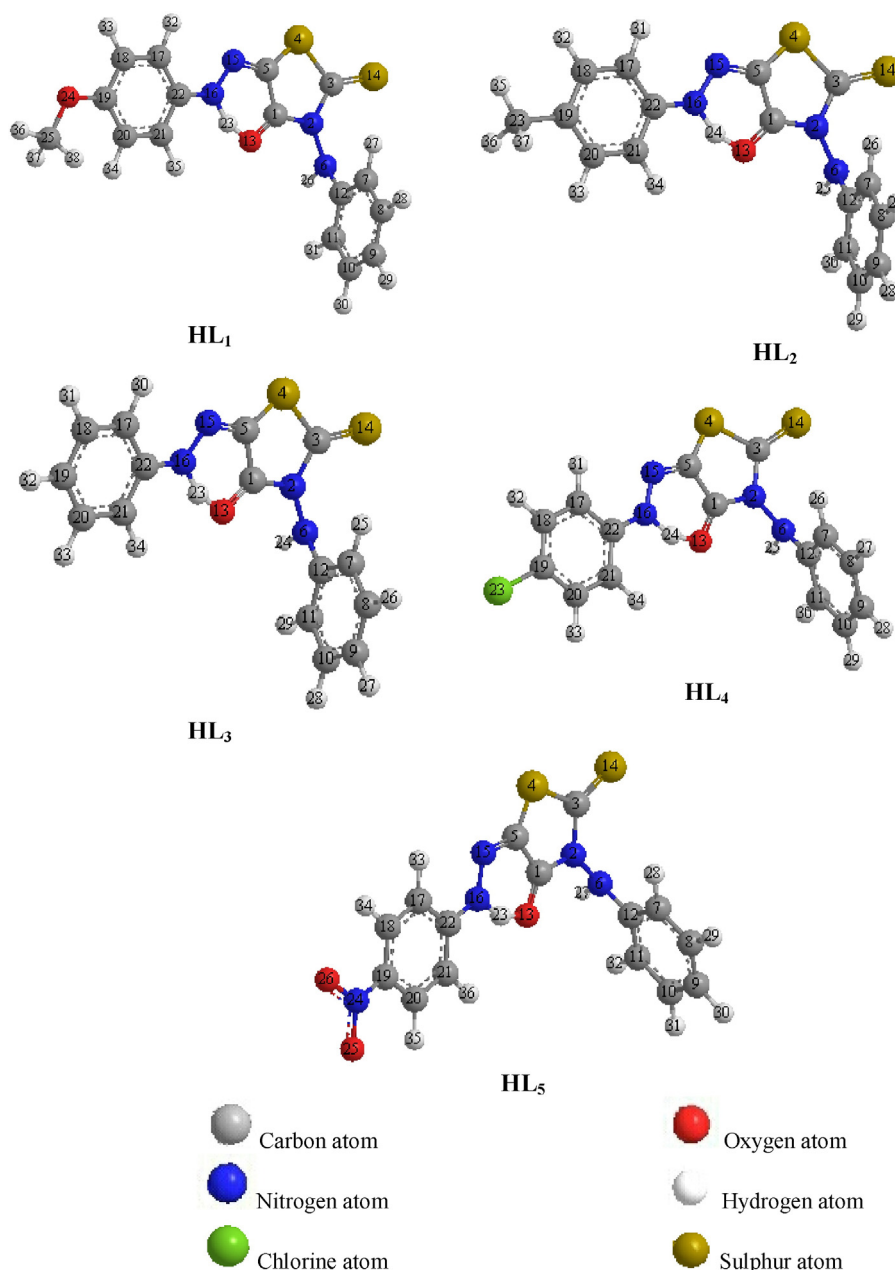


Fig. 3. The molecular structures for HL_n .

Table 2
The selected geometric parameters for HL₁.

Bond lengths (Å)		Bond angles (°)		Bond angles (°)	
C(25)–H(38)	1.113	H(38)–C(25)–H(37)	111.887	C(11)–C(12)–N(6)	118.424
C(25)–H(37)	1.113	H(38)–C(25)–H(36)	108.169	H(26)–N(6)–C(12)	114.354
C(25)–H(36)	1.113	H(38)–C(25)–O(24)	110.347	H(26)–N(6)–N(2)	116.442
C(21)–H(35)	1.104	H(37)–C(25)–H(36)	108.167	C(12)–N(6)–N(2)	122.051
C(20)–H(34)	1.102	H(37)–C(25)–O(24)	110.354	S(14)–C(3)–S(4)	125.084
C(18)–H(33)	1.104	H(36)–C(25)–O(24)	107.776	S(14)–C(3)–N(2)	129.758
C(17)–H(32)	1.103	C(19)–O(24)–C(25)	118.767	S(4)–C(3)–N(2)	105.156
C(11)–H(31)	1.104	H(34)–C(20)–C(21)	116.943	O(13)–H(23)–N(16)	154.903
C(10)–H(30)	1.103	H(34)–C(20)–C(19)	120.926	N(6)–N(2)–C(3)	125.249
C(9)–H(29)	1.103	C(21)–C(20)–C(19)	122.131	N(6)–N(2)–C(1)	123.904
C(8)–H(28)	1.103	C(20)–C(19)–C(18)	115.683	C(3)–N(2)–C(1)	110.84
C(7)–H(27)	1.103	C(20)–C(19)–O(24)	125.543	H(23)–O(13)–C(1)	108.968
N(6)–H(26)	1.051	C(18)–C(19)–O(24)	118.775	N(15)–C(5)–C(1)	116.374
C(17)–C(22)	1.345	H(33)–C(18)–C(19)	118.575	N(15)–C(5)–S(4)	131.246
C(21)–C(22)	1.345	H(33)–C(18)–C(17)	118.627	C(1)–C(5)–S(4)	112.38
C(20)–C(21)	1.343	C(19)–C(18)–C(17)	122.798	O(13)–C(1)–C(5)	115.027
C(19)–C(20)	1.348	H(35)–C(21)–C(22)	120.437	O(13)–C(1)–N(2)	129.783
C(18)–C(19)	1.347	H(35)–C(21)–C(20)	118.181	C(5)–C(1)–N(2)	115.187
C(17)–C(18)	1.342	C(22)–C(21)–C(20)	121.382	Dihedral angle (°)	
C(7)–C(12)	1.346	H(32)–C(17)–C(22)	121.128	C(18)–C(17)–C(22)–N(16)	179.997
C(11)–C(12)	1.345	H(32)–C(17)–C(18)	118.067	C(20)–C(21)–C(22)–N(16)	–179.99
C(10)–C(11)	1.342	C(22)–C(17)–C(18)	120.805	C(8)–C(7)–C(12)–N(6)	179.986
C(9)–C(10)	1.342	C(17)–C(22)–C(21)	117.202	C(10)–C(11)–C(12)–N(6)	–179.988
C(8)–C(9)	1.342	C(17)–C(22)–N(16)	122.386	C(7)–C(12)–N(6)–N(2)	–32.896
C(7)–C(8)	1.342	C(21)–C(22)–N(16)	120.412	N(15)–C(5)–C(1)–N(2)	–179.655
H(23)–O(13)	1.003	H(23)–N(16)–C(22)	122.189		
N(16)–H(23)	1.037	H(23)–N(16)–N(15)	108.605		
C(22)–N(16)	1.273	C(22)–N(16)–N(15)	129.206		
N(15)–N(16)	1.249	C(5)–S(4)–C(3)	96.437		
C(12)–N(6)	1.272	N(16)–N(15)–C(5)	116.122		
N(2)–N(6)	1.351	H(30)–C(10)–C(11)	120.035		
C(19)–O(24)	1.375	H(30)–C(10)–C(9)	119.886		
C(5)–N(15)	1.281	C(11)–C(10)–C(9)	120.079		
C(3)–S(4)	1.575	H(29)–C(9)–C(10)	120.144		
C(1)–O(13)	1.221	H(29)–C(9)–C(8)	120.146		
C(5)–C(1)	1.377	C(10)–C(9)–C(8)	119.709		
S(4)–C(5)	1.479	H(28)–C(8)–C(9)	119.865		
C(3)–S(4)	1.794	H(28)–C(8)–C(7)	120.019		
N(2)–C(3)	1.374	C(9)–C(8)–C(7)	120.116		
C(1)–N(2)	1.374	H(31)–C(11)–C(12)	120.723		
O(24)–C(25)	1.409	H(31)–C(11)–C(10)	118.691		
		C(12)–C(11)–C(10)	120.586		
		H(27)–C(7)–C(12)	121.023		
		H(27)–C(7)–C(8)	118.446		
		C(12)–C(7)–C(8)	120.531		
		C(7)–C(12)–C(11)	118.978		
		C(7)–C(12)–N(6)	122.597		

Table 3
The selected geometric parameters for HL₂.

Bond lengths (Å)		Bond angles (°)		Bond angles (°)	
C(23)–H(37)	1.114	H(37)–C(23)–H(36)	108.481	H(25)–N(6)–C(12)	114.364
C(23)–H(36)	1.114	H(37)–C(23)–H(35)	107.466	H(25)–N(6)–N(2)	116.46
C(23)–H(35)	1.113	H(37)–C(23)–C(19)	110.299	C(12)–N(6)–N(2)	122.051
C(21)–H(34)	1.104	H(36)–C(23)–H(35)	107.519	S(14)–C(3)–S(4)	125.08
C(20)–H(33)	1.103	H(36)–C(23)–C(19)	110.261	S(14)–C(3)–N(2)	129.763
C(18)–H(32)	1.103	H(35)–C(23)–C(19)	112.668	S(4)–C(3)–N(2)	105.156
C(17)–H(31)	1.103	H(33)–C(20)–C(21)	119.462	O(13)–H(24)–N(16)	154.915
C(11)–H(30)	1.104	H(33)–C(20)–C(19)	119.492	N(6)–N(2)–C(3)	125.252
C(10)–H(29)	1.103	C(21)–C(20)–C(19)	121.045	N(6)–N(2)–C(1)	123.907
C(9)–H(28)	1.103	C(20)–C(19)–C(18)	118.008	C(3)–N(2)–C(1)	110.834
C(8)–H(27)	1.103	C(20)–C(19)–C(23)	120.302	H(24)–O(13)–C(1)	108.969
C(7)–H(26)	1.103	C(18)–C(19)–C(23)	121.69	N(15)–C(5)–C(1)	116.371
N(6)–H(25)	1.051	H(32)–C(18)–C(19)	119.877	N(15)–C(5)–S(4)	131.248
C(17)–C(22)	1.346	H(32)–C(18)–C(17)	119.118	C(1)–C(5)–S(4)	112.381
C(21)–C(22)	1.346	C(19)–C(18)–C(17)	121.006	O(13)–C(1)–C(5)	115.024
C(20)–C(21)	1.342	H(34)–C(21)–C(22)	120.811	O(13)–C(1)–N(2)	129.783
C(19)–C(20)	1.344	H(34)–C(21)–C(20)	118.114	C(5)–C(1)–N(2)	115.191
C(18)–C(19)	1.344	C(22)–C(21)–C(20)	121.075	Dihedral angle (°)	
C(17)–C(18)	1.343	H(31)–C(17)–C(22)	121.077	C(18)–C(17)–C(22)–N(16)	–179.998
C(7)–C(12)	1.346	H(31)–C(17)–C(18)	117.833	C(20)–C(21)–C(22)–N(16)	–179.998
C(11)–C(12)	1.345	C(22)–C(17)–C(18)	121.09	C(8)–C(7)–C(12)–N(6)	179.979

Table 3 (continued)

Bond lengths (Å)		Bond angles (°)		Bond angles (°)	
C(10)–C(11)	1.342	C(17)–C(22)–C(21)	117.775	C(10)–C(11)–C(12)–N(6)	–179.979
C(9)–C(10)	1.342	C(17)–C(22)–N(16)	122.127	C(7)–C(12)–N(6)–N(2)	–32.812
C(8)–C(9)	1.342	C(21)–C(22)–N(16)	120.097	N(15)–C(5)–C(1)–N(2)	–179.688
C(7)–C(8)	1.342	H(24)–N(16)–C(22)	122.19		
H(24)–O(13)	1.004	H(24)–N(16)–N(15)	108.581		
N(16)–H(24)	1.037	C(22)–N(16)–N(15)	129.228		
C(22)–N(16)	1.274	C(5)–S(4)–C(3)	96.438		
N(15)–N(16)	1.249	N(16)–N(15)–C(5)	116.139		
C(12)–N(6)	1.272	H(29)–C(10)–C(11)	120.036		
N(2)–N(6)	1.351	H(29)–C(10)–C(9)	119.883		
C(19)–C(23)	1.51	C(11)–C(10)–C(9)	120.081		
C(5)–N(15)	1.281	H(28)–C(9)–C(10)	120.147		
C(3)–S(14)	1.575	H(28)–C(9)–C(8)	120.145		
C(1)–O(13)	1.221	C(10)–C(9)–C(8)	119.708		
C(5)–C(1)	1.377	H(27)–C(8)–C(9)	119.867		
S(4)–C(5)	1.479	H(27)–C(8)–C(7)	120.016		
C(3)–S(4)	1.794	C(9)–C(8)–C(7)	120.117		
N(2)–C(3)	1.374	H(30)–C(11)–C(12)	120.723		
C(1)–N(2)	1.374	H(30)–C(11)–C(10)	118.695		
		C(12)–C(11)–C(10)	120.581		
		H(26)–C(7)–C(12)	121.026		
		H(26)–C(7)–C(8)	118.444		
		C(12)–C(7)–C(8)	120.53		
		C(7)–C(12)–C(11)	118.981		
		C(7)–C(12)–N(6)	122.586		
		C(11)–C(12)–N(6)	118.431		

Table 4

The selected geometric parameters for HL₃.

Bond lengths (Å)		Bond angles (°)		Bond angles (°)	
C(21)–H(34)	1.104	H(33)–C(20)–C(21)	120.073	O(13)–H(23)–N(16)	154.932
C(20)–H(33)	1.103	H(33)–C(20)–C(19)	119.833	N(6)–N(2)–C(3)	125.247
C(19)–H(32)	1.103	C(21)–C(20)–C(19)	120.094	N(6)–N(2)–C(1)	123.915
C(18)–H(31)	1.103	H(32)–C(19)–C(20)	120.261	C(3)–N(2)–C(1)	110.831
C(17)–H(30)	1.103	H(32)–C(19)–C(18)	120.264	H(23)–O(13)–C(1)	108.97
C(11)–H(29)	1.104	C(20)–C(19)–C(18)	119.475	N(15)–C(5)–C(1)	116.365
C(10)–H(28)	1.103	H(31)–C(18)–C(19)	119.779	N(15)–C(5)–S(4)	131.255
C(9)–H(27)	1.103	H(31)–C(18)–C(17)	120.051	C(1)–C(5)–S(4)	112.381
C(8)–H(26)	1.103	C(19)–C(18)–C(17)	120.17	O(13)–C(1)–C(5)	115.021
C(7)–H(25)	1.103	H(34)–C(21)–C(22)	120.84	O(13)–C(1)–N(2)	129.784
N(6)–H(24)	1.051	H(34)–C(21)–C(20)	118.03	C(5)–C(1)–N(2)	115.192
C(17)–C(22)	1.347	C(22)–C(21)–C(20)	121.13	Dihedral angle (°)	
C(21)–C(22)	1.347	H(30)–C(17)–C(22)	121.177	C(18)–C(17)–C(22)–N(16)	179.985
C(20)–C(21)	1.342	H(30)–C(17)–C(18)	117.779	C(20)–C(21)–C(22)–N(16)	–179.985
C(19)–C(20)	1.341	C(22)–C(17)–C(18)	121.044	C(8)–C(7)–C(12)–N(6)	179.987
C(18)–C(19)	1.341	C(17)–C(22)–C(21)	118.088	C(10)–C(11)–C(12)–N(6)	–179.978
C(17)–C(18)	1.343	C(17)–C(22)–N(16)	121.969	C(7)–C(12)–N(6)–N(2)	–32.818
C(7)–C(12)	1.346	C(21)–C(22)–N(16)	119.943	N(15)–C(5)–C(1)–N(2)	–179.634
C(11)–C(12)	1.345	H(23)–N(16)–C(22)	122.183		
C(10)–C(11)	1.342	H(23)–N(16)–N(15)	108.56		
C(9)–C(10)	1.342	C(22)–N(16)–N(15)	129.257		
C(8)–C(9)	1.342	C(5)–S(4)–C(3)	96.436		
C(7)–C(8)	1.342	N(16)–N(15)–C(5)	116.153		
H(23)–O(13)	1.003	H(28)–C(10)–C(11)	120.033		
N(16)–H(23)	1.037	H(28)–C(10)–C(9)	119.886		
C(22)–N(16)	1.274	C(11)–C(10)–C(9)	120.081		
N(15)–N(16)	1.249	H(27)–C(9)–C(10)	120.146		
C(12)–N(6)	1.272	H(27)–C(9)–C(8)	120.15		
N(2)–N(6)	1.351	C(10)–C(9)–C(8)	119.704		
C(5)–N(15)	1.281	H(26)–C(8)–C(9)	119.864		
C(3)–S(14)	1.575	H(26)–C(8)–C(7)	120.017		
C(1)–O(13)	1.221	C(9)–C(8)–C(7)	120.119		
C(5)–C(1)	1.377	H(29)–C(11)–C(12)	120.724		
S(4)–C(5)	1.479	H(29)–C(11)–C(10)	118.692		
C(3)–S(4)	1.794	C(12)–C(11)–C(10)	120.584		
N(2)–C(3)	1.374	H(25)–C(7)–C(12)	121.023		
C(1)–N(2)	1.374	H(25)–C(7)–C(8)	118.448		
		C(12)–C(7)–C(8)	120.529		
		C(7)–C(12)–C(11)	118.98		
		C(7)–C(12)–N(6)	122.597		
		C(11)–C(12)–N(6)	118.422		

(continued on next page)

Table 4 (continued)

Bond lengths (Å)	Bond angles (°)	Bond angles (°)
	H(24)–N(6)–C(12)	114.354
	H(24)–N(6)–N(2)	116.459
	C(12)–N(6)–N(2)	122.069
	S(14)–C(3)–S(4)	125.08
	S(14)–C(3)–N(2)	129.76
	S(4)–C(3)–N(2)	105.159

salmon sperm DNA binding activity of the ligands (**HL_n**) was studied by absorption spectra measurements.

2. Experimental

2.1. Materials

3-Phenylamino-2-thioxothiazolidin-4-one was prepared previously [1,8,13]. The standard chemical cobalt acetate, aniline and 4-alkylanilines (alkyl: CH₃, OCH₃, Cl and NO₂) were purchased from Sigma and Aldrich and used without any further purification. Salmon

sperm DNA (SS-DNA) was purchased from SRL (India). Double distilled water was used to prepare all buffer solutions.

2.2. Preparation of azodye ligands

Preparation of 5-(4'-alkylphenylazo)-3-phenylamino-2-thioxothiazolidin-4-one (**HL_n**) (Fig. 1); 25 ml of distilled water containing hydrochloric acid was added to aniline or a 4-alkyl-aniline. To the resulting mixture stirred and cooled to 0 °C, a solution of sodium nitrite 0.01 mol in 20 ml of water was added dropwise. The formed diazonium chloride was consecutively coupled with an alkaline solution of 3-phenylamino-2-thioxothiazolidin-4-one 0.01 mol in 10 ml of pyridine.

Table 5

The selected geometric parameters for **HL₄**.

Bond lengths (Å)	Bond angles (°)	Bond angles (°)			
C(21)–H(34)	1.104	H(33)–C(20)–C(21)	119.374	O(13)–H(24)–N(16)	154.955
C(20)–H(33)	1.103	H(33)–C(20)–C(19)	120.663	N(6)–N(2)–C(3)	125.246
C(18)–H(32)	1.103	C(21)–C(20)–C(19)	119.962	N(6)–N(2)–C(1)	123.92
C(17)–H(31)	1.103	C(20)–C(19)–C(18)	119.575	C(3)–N(2)–C(1)	110.827
C(11)–H(30)	1.104	C(20)–C(19)–Cl(23)	120.223	H(24)–O(13)–C(1)	108.971
C(10)–H(29)	1.103	C(18)–C(19)–Cl(23)	120.201	N(15)–C(5)–C(1)	116.366
C(9)–H(28)	1.103	H(32)–C(18)–C(19)	120.612	N(15)–C(5)–S(4)	131.251
C(8)–H(27)	1.103	H(32)–C(18)–C(17)	119.34	C(1)–C(5)–S(4)	112.383
C(7)–H(26)	1.103	C(19)–C(18)–C(17)	120.048	O(13)–C(1)–C(5)	115.007
N(6)–H(25)	1.051	H(34)–C(21)–C(22)	120.75	O(13)–C(1)–N(2)	129.797
C(17)–C(22)	1.347	H(34)–C(21)–C(20)	118.006	C(5)–C(1)–N(2)	115.194
C(21)–C(22)	1.347	C(22)–C(21)–C(20)	121.244	Dihedral angle (°)	
C(20)–C(21)	1.343	H(31)–C(17)–C(22)	121.082	C(18)–C(17)–C(22)–N(16)	–179.999
C(19)–C(20)	1.342	H(31)–C(17)–C(18)	117.768	C(20)–C(21)–C(22)–N(16)	180
C(18)–C(19)	1.342	C(22)–C(17)–C(18)	121.149	C(8)–C(7)–C(12)–N(6)	179.984
C(17)–C(18)	1.343	C(17)–C(22)–C(21)	118.021	C(10)–C(11)–C(12)–N(6)	–179.986
C(7)–C(12)	1.346	C(17)–C(22)–N(16)	122.004	C(7)–C(12)–N(6)–N(2)	–32.136
C(11)–C(12)	1.345	C(21)–C(22)–N(16)	119.975	N(15)–C(5)–C(1)–N(2)	–179.659
C(10)–C(11)	1.342	H(24)–N(16)–C(22)	122.169		
C(9)–C(10)	1.342	H(24)–N(16)–N(15)	108.541		
C(8)–C(9)	1.342	C(22)–N(16)–N(15)	129.289		
C(7)–C(8)	1.342	C(5)–S(4)–C(3)	96.431		
H(24)–O(13)	1.003	N(16)–N(15)–C(5)	116.159		
N(16)–H(24)	1.037	H(29)–C(10)–C(11)	120.04		
C(22)–N(16)	1.274	H(29)–C(10)–C(9)	119.885		
N(15)–N(16)	1.249	C(11)–C(10)–C(9)	120.075		
C(12)–N(6)	1.272	H(28)–C(9)–C(10)	120.144		
N(2)–N(6)	1.351	H(28)–C(9)–C(8)	120.152		
C(19)–Cl(23)	1.727	C(10)–C(9)–C(8)	119.705		
C(5)–N(15)	1.281	H(27)–C(8)–C(9)	119.863		
C(3)–S(14)	1.575	H(27)–C(8)–C(7)	120.012		
C(1)–O(13)	1.221	C(9)–C(8)–C(7)	120.125		
C(5)–C(1)	1.377	H(30)–C(11)–C(12)	120.723		
S(4)–C(5)	1.479	H(30)–C(11)–C(10)	118.682		
C(3)–S(4)	1.794	C(12)–C(11)–C(10)	120.594		
N(2)–C(3)	1.374	H(26)–C(7)–C(12)	121.032		
C(1)–N(2)	1.374	H(26)–C(7)–C(8)	118.439		
		C(12)–C(7)–C(8)	120.528		
		C(7)–C(12)–C(11)	118.971		
		C(7)–C(12)–N(6)	122.624		
		C(11)–C(12)–N(6)	118.403		
		H(25)–N(6)–C(12)	114.435		
		H(25)–N(6)–N(2)	116.559		
		C(12)–N(6)–N(2)	122.197		
		S(14)–C(3)–S(4)	125.075		
		S(14)–C(3)–N(2)	129.759		
		S(4)–C(3)–N(2)	105.166		

The colored precipitate, which formed immediately, was filtered and washed several times with water. The crude product was purified by recrystallization from hot ethanol [7]. The analytical data confirmed the expected compositions (Table 1). The ligands (Fig. 1) were also characterized by ^1H NMR and IR spectroscopy.

The resulting formed ligands are:

HL1 = 5-(4'-methoxyphenylazo)-3-phenylamino-2-thioxothiazolidin-4-one.

HL2 = 5-(4'-methylphenylazo)-3-phenylamino-2-thioxothiazolidin-4-one.

HL3 = 5-(phenylazo)-3-phenylamino-2-thioxothiazolidin-4-one.

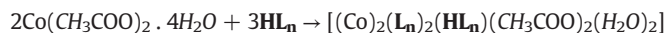
HL4 = 5-(4'-chlorophenylazo)-3-phenylamino-2-thioxothiazolidin-4-one.

HL5 = 5-(4'-nitrophenylazo)-3-phenylamino-2-thioxothiazolidin-4-one.

2.3. Preparation of Co(II) complexes

All Co(II) polymer complexes were synthesized according to the general procedure [7]: a stoichiometric amount of the desired ligand

(0.03 mol) in EtOH (20 cm³) was added dropwise to a hot EtOH solution (20 cm³) of Co(CH₃COO)₂·4H₂O (0.02 mol) with stirring and the reaction mixture was refluxed for 3 h. The solution was concentrated to half of its original volume by evaporation and allowed to cool at room temperature. During this, a polycrystalline solid was separated, which was isolated by filtration, washed with EtOH, ether and dried *in vacuo* over anhydrous CaCl₂. Formation of the polymer complexes (Fig. 2) can be obtainable in the following reaction:



2.4. Measurements

Microanalytical data (C, H and N) were collected on Automatic Analyzer CHNS Vario ELIII, Germany. Spectroscopic data were obtained using the following instruments: FT-IR spectra (KBr disks, 4000–400 cm⁻¹) by Jasco FTIR-4100 spectrophotometer; the ^1H -NMR spectra by Bruker WP 300 MHz using DMSO-d₆ as a solvent containing TMS as the internal standard. X-ray diffraction analysis of compounds in powder forms was recorded on X-ray diffractometer in the range of diffraction angle $2\theta = 4\text{--}80^\circ$. This analysis was carried out using CuK α

Table 6

The selected geometric parameters for HL₅.

Bond lengths (Å)		Bond angles (°)		Bond angles (°)	
C(21)–H(36)	1.104	C(19)–N(24)–O(26)	123.194	S(14)–C(3)–S(4)	125.137
C(20)–H(35)	1.104	C(19)–N(24)–O(25)	123.277	S(14)–C(3)–N(2)	129.758
C(18)–H(34)	1.104	O(26)–N(24)–O(25)	113.529	S(4)–C(3)–N(2)	105.104
C(17)–H(33)	1.104	H(35)–C(20)–C(21)	117.229	O(13)–H(23)–N(16)	154.405
C(11)–H(32)	1.104	H(35)–C(20)–C(19)	120.927	N(6)–N(2)–C(3)	125.155
C(10)–H(31)	1.103	C(21)–C(20)–C(19)	121.844	N(6)–N(2)–C(1)	123.876
C(9)–H(30)	1.103	C(20)–C(19)–C(18)	116.528	C(3)–N(2)–C(1)	110.964
C(8)–H(29)	1.103	C(20)–C(19)–N(24)	122.139	H(23)–O(13)–C(1)	108.934
C(7)–H(28)	1.103	C(18)–C(19)–N(24)	121.333	N(15)–C(5)–C(1)	116.031
N(6)–H(27)	1.051	H(34)–C(18)–C(19)	121.134	N(15)–C(5)–S(4)	131.371
C(17)–C(22)	1.346	H(34)–C(18)–C(17)	117.124	C(1)–C(5)–S(4)	112.597
C(21)–C(22)	1.345	C(19)–C(18)–C(17)	121.742	O(13)–C(1)–C(5)	115.476
C(20)–C(21)	1.344	H(36)–C(21)–C(22)	120.232	O(13)–C(1)–N(2)	129.532
C(19)–C(20)	1.348	H(36)–C(21)–C(20)	118.425	C(5)–C(1)–N(2)	114.989
C(18)–C(19)	1.347	C(22)–C(21)–C(20)	121.342	Dihedral angle (°)	
C(17)–C(18)	1.343	H(33)–C(17)–C(22)	121.014	C(18)–C(17)–C(22)–N(16)	–179.933
C(7)–C(12)	1.346	H(33)–C(17)–C(18)	117.472	C(20)–C(21)–C(22)–N(16)	179.94
C(11)–C(12)	1.345	C(22)–C(17)–C(18)	121.514	C(8)–C(7)–C(12)–N(6)	179.976
C(10)–C(11)	1.342	C(17)–C(22)–C(21)	117.03	C(10)–C(11)–C(12)–N(6)	–179.978
C(9)–C(10)	1.342	C(17)–C(22)–N(16)	121.919	C(7)–C(12)–N(6)–N(2)	–33.186
C(8)–C(9)	1.342	C(21)–C(22)–N(16)	121.05	N(15)–C(5)–C(1)–N(2)	–179.523
C(7)–C(8)	1.342	H(23)–N(16)–C(22)	123.452		
H(23)–O(13)	1.005	H(23)–N(16)–N(15)	108.738		
N(16)–H(23)	1.038	C(22)–N(16)–N(15)	127.808		
C(22)–N(16)	1.275	C(5)–S(4)–C(3)	96.346		
N(15)–N(16)	1.25	N(16)–N(15)–C(5)	116.416		
C(12)–N(6)	1.272	H(31)–C(10)–C(11)	120.034		
N(2)–N(6)	1.351	H(31)–C(10)–C(9)	119.885		
C(19)–N(24)	1.259	C(11)–C(10)–C(9)	120.082		
C(5)–N(15)	1.28	H(30)–C(9)–C(10)	120.148		
C(3)–S(4)	1.575	H(30)–C(9)–C(8)	120.143		
C(1)–O(13)	1.221	C(10)–C(9)–C(8)	119.71		
C(5)–C(1)	1.376	H(29)–C(8)–C(9)	119.872		
S(4)–C(5)	1.479	H(29)–C(8)–C(7)	120.012		
C(3)–S(4)	1.794	C(9)–C(8)–C(7)	120.116		
N(2)–C(3)	1.374	H(32)–C(11)–C(12)	120.726		
C(1)–N(2)	1.375	H(32)–C(11)–C(10)	118.697		
N(24)–O(26)	1.316	C(12)–C(11)–C(10)	120.577		
N(24)–O(25)	1.315	H(28)–C(7)–C(12)	121.017		
		H(28)–C(7)–C(8)	118.457		
		C(12)–C(7)–C(8)	120.526		
		C(7)–C(12)–C(11)	118.988		
		C(7)–C(12)–N(6)	122.567		
		C(11)–C(12)–N(6)	118.445		
		H(27)–N(6)–C(12)	114.324		
		H(27)–N(6)–N(2)	116.416		
		C(12)–N(6)–N(2)	121.983		

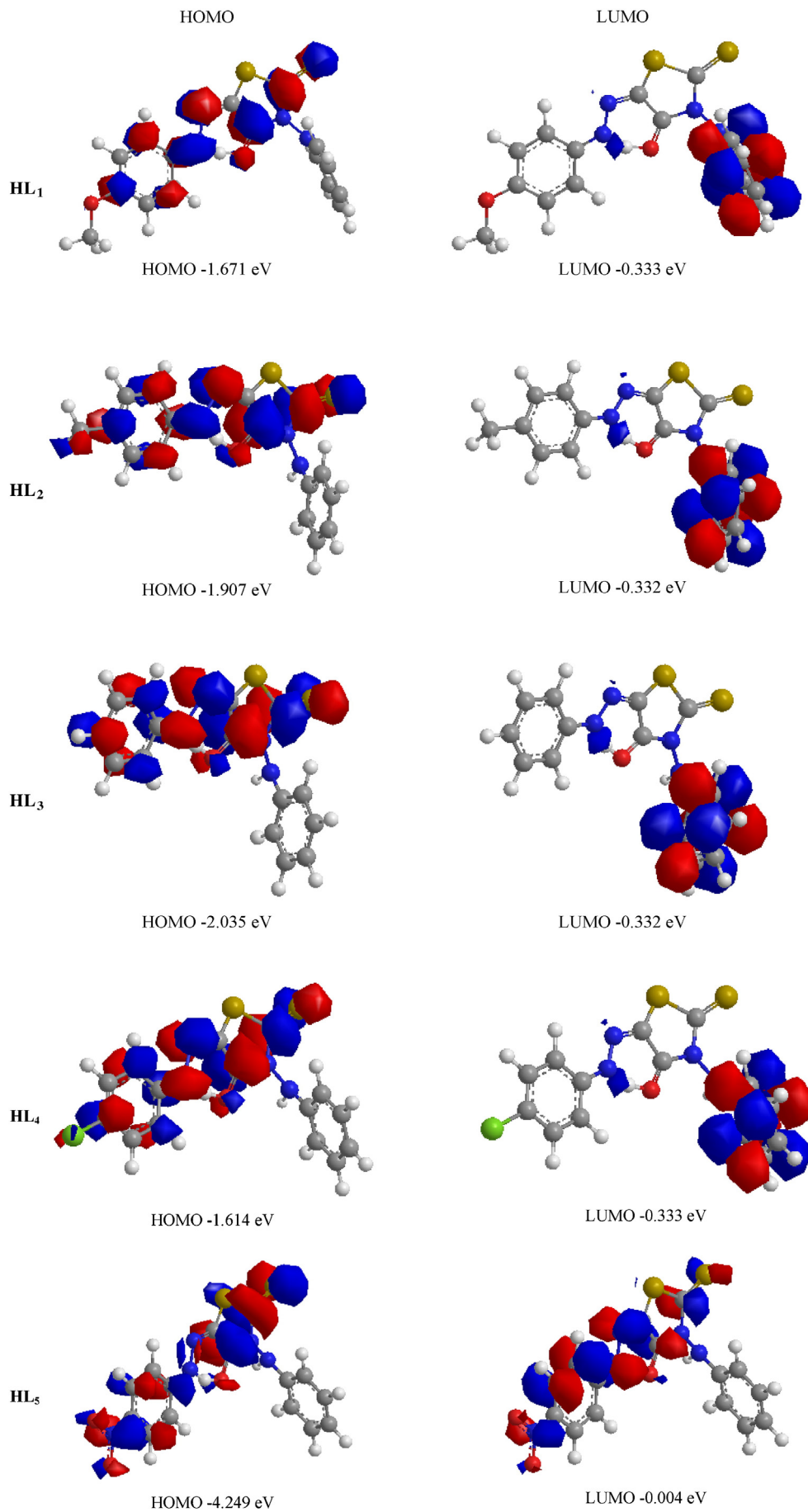
Fig. 4. The molecular structures (HOMO & LUMO) for HL_n.

Table 7The calculated quantum chemical parameters for the ligands (**HL_n**).

Comp.	E _{HOMO} (eV)	E _{LUMO} (eV)	ΔE (eV)	χ (eV)	η (eV)	σ (eV) ⁻¹	Pi (eV)	S (eV) ⁻¹	ω (eV)	ΔN _{max}
HL₁	-1.671	-0.333	1.338	1.002	0.669	1.49476831	-1.002	0.74738416	0.75037668	1.49775785
HL₂	-1.907	-0.332	1.575	1.1195	0.7875	1.26984127	-1.1195	0.63492063	0.79573349	1.4215873
HL₃	-2.035	-0.332	1.703	1.1835	0.8515	1.17439812	-1.1835	0.58719906	0.82247343	1.38990018
HL₄	-1.614	-0.333	1.281	0.9735	0.6405	1.56128025	-0.9735	0.78064012	0.7398144	1.51990632
HL₅	-4.249	-0.004	4.245	2.1265	2.1225	0.47114252	-2.1265	0.23557126	1.06525377	1.00188457

radiation ($\lambda = 1.540598 \text{ \AA}$). The applied voltage and the tube current are 40 KV and 30 mA, respectively. Mass spectra were recorded by the EI technique at 70 eV using MS-5988 GS-MS Hewlett-Packard. UV-Visible spectra by Perkin-Elmer AA800 spectrophotometer Model AAS. Thermal analysis of the ligands and their Co (II) complexes was carried out using a Shimadzu thermogravimetric analyzer under a nitrogen atmosphere with heating rate of 10 °C/min over a temperature range from 30 °C up to 800 °C. Magnetic susceptibility measurements were determined at room temperature on a Johnson Matthey magnetic susceptibility balance using Hg[Co(SCN)₄] as calibrate. Conductivity measurements of the complexes at $25 \pm 1 \text{ }^\circ\text{C}$ were determined in DMF (10^{-3} M) using conductivity/TDS meter model Lutron YK-22CT. The molecular structures of the investigated compounds were optimized by HF method with 3-21G basis set. The molecules were built with the Perkin Elmer ChemBio Draw and optimized using Perkin Elmer ChemBio3D software [18,19].

2.5. DNA binding experiments

The binding properties of the ligands and their complexes to SS-DNA have been studied using electronic absorption spectroscopy. SS-DNA (50 mg) was dissolved by stirring overnight in double deionized water (pH = 7.0) and kept at 4 °C. Doubly distilled water was used to prepare buffers (20 mM phosphate buffer (NaH₂PO₄-Na₂HPO₄), pH = 7.2). A solution of (SS-DNA) in the buffer gave a ratio of UV absorbance at 260 and 280 nm (A_{260}/A_{280}) of ca. 1.8, indicating that the DNA was sufficiently free of protein [20]. The DNA concentration was determined by UV absorbance spectroscopy using the molar absorption coefficient of $6600 \text{ M}^{-1} \text{ cm}^{-1}$ at 260 nm for SS-DNA [21,22] and was found to be 1.4×10^{-4} . Electronic absorption spectra (200–900 nm) were carried out using 1 cm quartz cuvette at 25 °C by fixing the concentration of ligand ($1.00 \times 10^{-3} \text{ mol.L}^{-1}$), while gradually increasing the concentration of SS-DNA (0.00 to $1.30 \times 10^{-4} \text{ mol.L}^{-1}$). An equal amount of SS-DNA was added to both the compound solutions and the references

buffer solution to eliminate the absorbance of SS-DNA itself. The intrinsic binding constant K_b of the compound with SS-DNA was determined using the following Eq. (1) [23]:

$$[\text{DNA}] / (\epsilon_a - \epsilon_f) = [\text{DNA}] / (\epsilon_b - \epsilon_f) + 1 / K_b (\epsilon_a - \epsilon_f) \quad (1)$$

where [DNA] is the concentration of SS-DNA in base pairs, ϵ_a is the extinction coefficient observed for the $A_{\text{obs}}/[\text{compound}]$ at the given DNA concentration, ϵ_f is the extinction coefficient of the free compound in solution and ϵ_b is the extinction coefficient of the compound when fully bond to DNA. In plots of $[\text{DNA}] / (\epsilon_a - \epsilon_f)$ vs. [DNA], K_b is given by the ratio of the slope to the intercept.

2.6. Cytotoxicity investigation

2.6.1. Cell lines and chemical reagents

Hepatocellular carcinoma (HePG-2) and mammary gland breast cancer (MCF-7) cell lines were obtained from ATCC via Holding company for biological products and vaccines (VACSERA), Cairo, Egypt. Chemical reagents; RPMI-1640 medium, MTT, DMSO and 5-fluorouracil were purchased from Sigma chemicals (St. Louis, USA), Fetal Bovine serum (FBS) was purchased from (GIBCO, UK). 5-fluorouracil (5-FU) was used as a standard anticancer drug for comparison.

2.6.2. MTT assay

The cell lines mentioned above were used to determine the inhibitory effects of ligands and their Co(II) complexes on cell growth using the MTT assay [24]. This colorimetric assay is based on the conversion of the yellow tetrazolium bromide (MTT) to a purple formazan derivative by mitochondrial succinate dehydrogenase in viable cells. Cell lines were cultured in RPMI-1640 medium with 10% fetal bovine serum. Antibiotics added were 100 units/ml penicillin and 100 μg/ml streptomycin at 37 °C in a 5% CO₂ incubator. The cell lines were seeded in a 96-well plate at a density of 1.0×10^4 cells/well at 37 °C for 48 h under 5% CO₂, followed by 24 h incubation with the indicated drug doses [25]. In the end of the drug treatment, 20 μl of MTT solution at 5 mg/ml was added and incubated for 4 h. Dimethyl sulfoxide (DMSO) in volume of 100 μl is added into each well to dissolve the purple formazan formed. The colorimetric assay is measured and recorded as absorbance at 570 nm using a plate reader (EXL 800). Cytotoxicity was expressed as

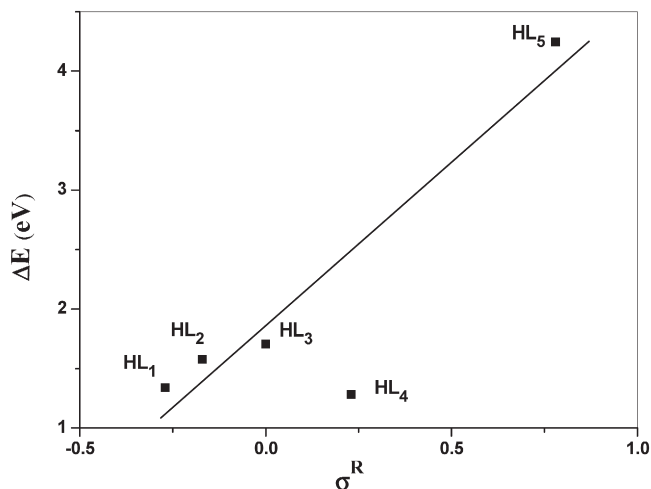


Fig. 5. The relation between Hammett's substitution coefficients (σ^R) vs. energy gap (ΔE).

Table 8IR data (cm^{-1}) of free ligands (**HL_n**) and their Co(II) complexes (**1–5**).

Compound	$\nu(\text{NH})$	$\nu(\text{C}=\text{O})$	$\nu(\text{C}=\text{S})$	$\nu(\text{Co}-\text{O})$	$\nu(\text{Co}-\text{N})$	$\nu(\text{Co}-\text{S})$
HL₁	3207	1751	881	–	–	–
(1)	–	1722	825	680	528	485
HL₂	3205	1754	882	–	–	–
(2)	–	1718	815	684	590	488
HL₃	3209	1727	842	–	–	–
(3)	–	1725	815	690	598	499
HL₄	3207	1751	823	–	–	–
(4)	–	1724	819	690	580	498
HL₅	3210	1735	846	–	–	–
(5)	–	1716	844	680	590	480

^aNumbers as given in Table 1.

IC₅₀ (µg/mL) which indicates the concentration of the compound that inhibited proliferation rate of the tumor cells by 50% as compared to the control untreated cells. IC₅₀ values were determined from the plot: % relative cell viability (% inhibition concentration) vs. compound concentration. The relative cell viability values were calculated as follows:

$$\% \text{The relative cell viability} = \frac{A(570 \text{ nm}) \text{ of treated samples}}{A(570 \text{ nm}) \text{ of untreated sample}} \times 100$$

2.7. Antioxidant investigation

Antioxidant activity screening assay ABTS method [26–28] used for determination of scavenging activity of ligands (HL_n) and their Co(II) complexes (1–5). For each of the investigated compounds (2 mL) of ABTS (2,2'-azinobis-(3-ethyl-benzothiazoline-6-sulphonic acid) solution (60 µM) was added to 3 mL MnO₂ solution (25 mg/mL), all prepared in (5 mL) aqueous phosphate buffer solution (pH 7, 0.1 M). The mixture was shaken, centrifuged, filtered and the absorbance of the resulting green blue solution (ABTS free radical solution) at 734 nm was adjusted to approx. ca. 0.5. Then, 50 µl of (2 mM) solution of the tested compound in spectroscopic grade MeOH/phosphate buffer (1:1) was added. The absorbance was measured and the reduction in color intensity was expressed as inhibition percentage (I %). Blank

sample was run without ABTS and using MeOH/phosphate buffer (1:1) instead of tested compounds. L-ascorbic acid was used as standard antioxidant (positive control) and the negative control was run with ABTS and MeOH/phosphate buffer (1:1) only.

$$\% \text{Inhibition} = \frac{A(\text{control}) - A(\text{test})}{A(\text{control})} \times 100$$

2.8. Antimicrobial investigation

Rhodanine compounds were individually tested against Gram negative (*Escherichia coli*) bacteria, Gram positive (*Staphylococcus aureus*) and yeast (*Candida albicans*). Each of the compounds was dissolved in DMSO and solutions of the concentration 1 mg/ml were prepared separately and paper disks of Whatman filter paper were prepared with standard size (5 cm) and sterilized in an autoclave. The paper disks were soaked in the desired concentration of the complex solution and were placed aseptically in the petri dishes containing nutrient agar media (agar 20 g, beef extract 3 g and peptone 5 g) seeded with *Staphylococcus aureus*, *E. coli* and *Candida albicans*. The petri dishes were incubated at 36 °C and the inhibition zones were recorded after 24 h of incubation. Each treatment was replicated three times. The antibacterial activity of a common standard antibiotic ampicillin and

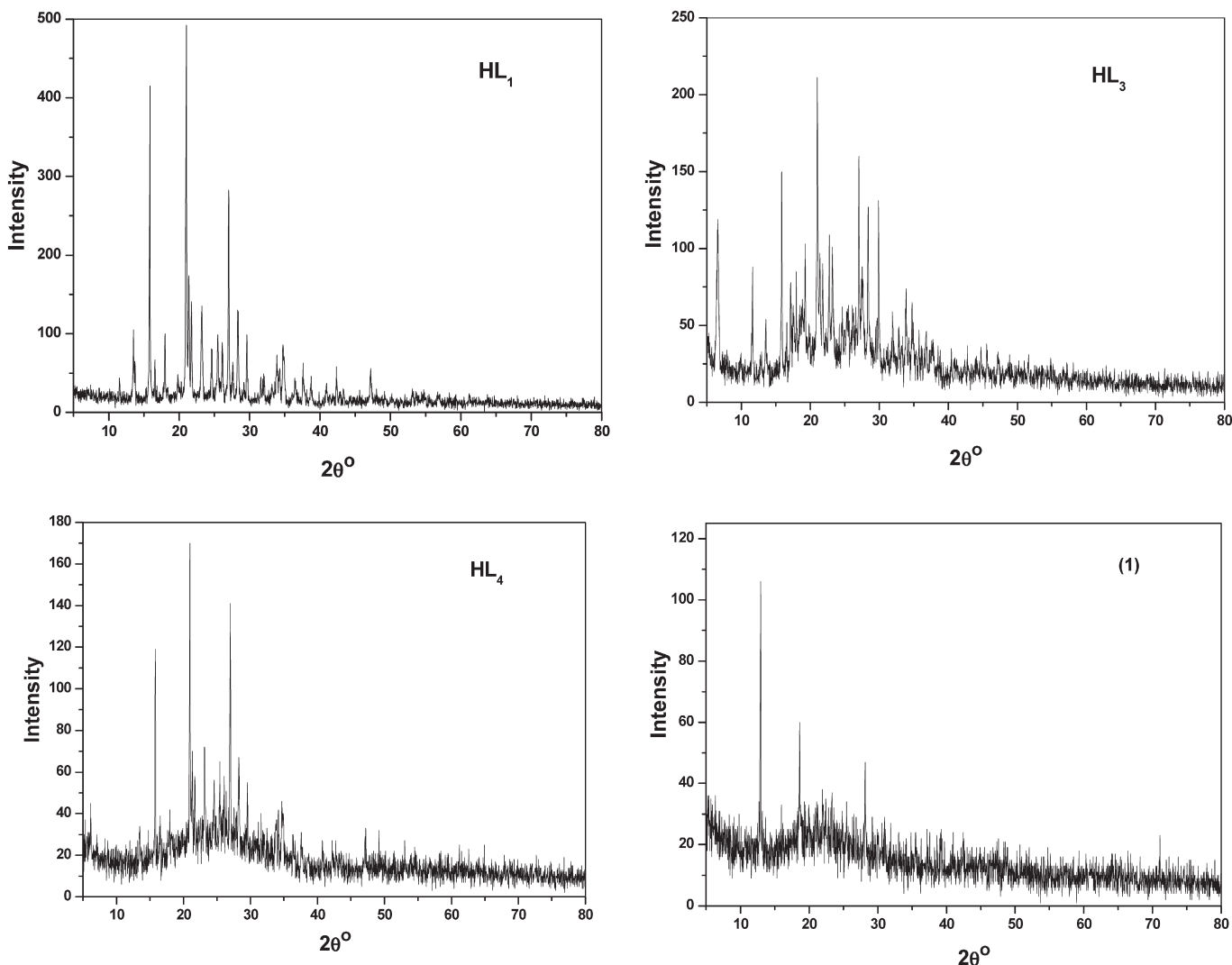


Fig. 6. X-ray diffraction patterns for ligands (HL₁, HL₃ and HL₄) and the complex (1) in powder forms.

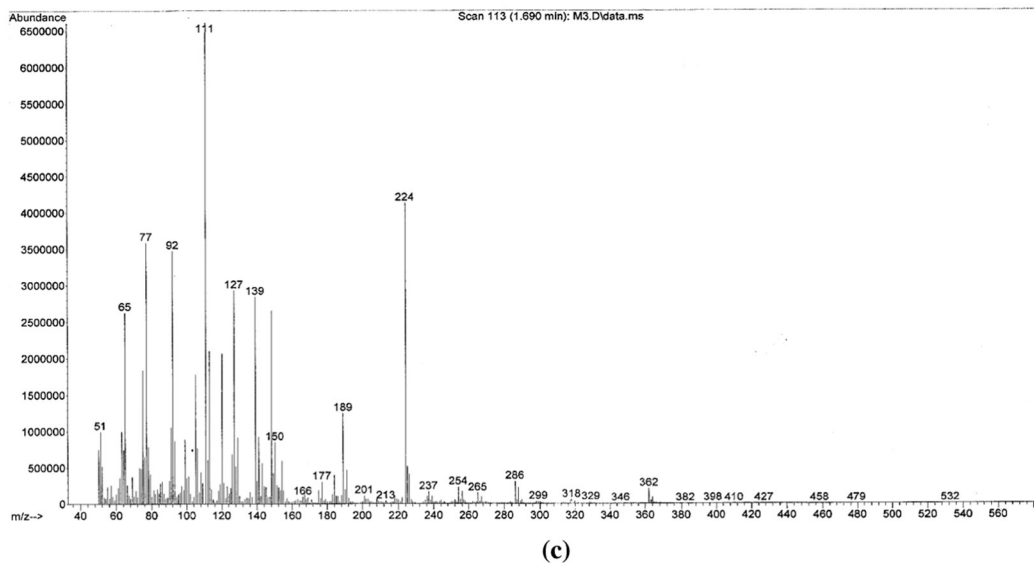
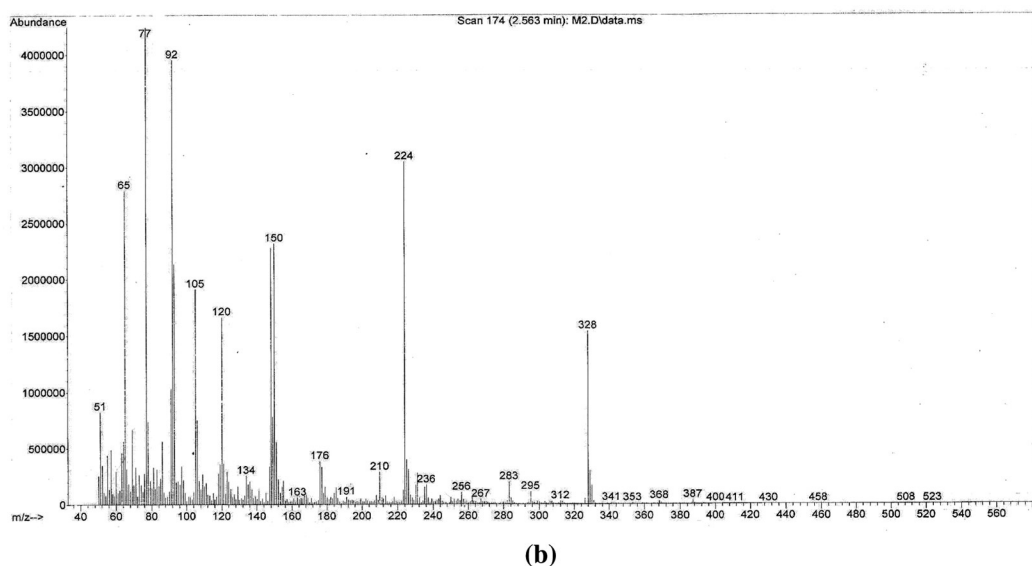
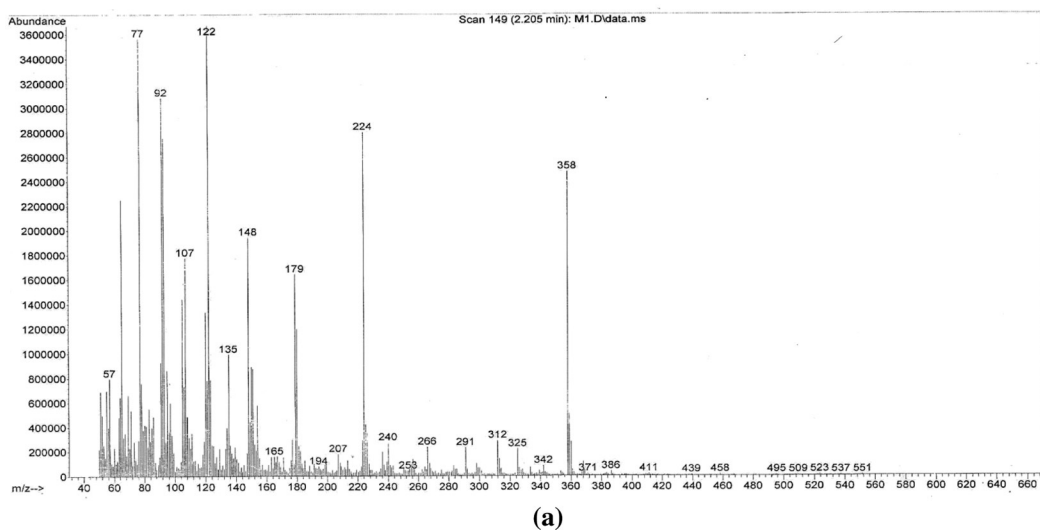


Fig. 7. a. Mass spectrum of HL₁. b. Mass spectrum of HL₃. c. Mass spectrum of HL₄.

antifungal colitrimazole was also recorded using the same procedure as above using the same concentration and solvents. The % activity index for the complex was calculated by the formula:

$$\% \text{Activity Index} = \frac{\text{Zone of inhibition by test compound (diameter)}}{\text{Zone of inhibition by standard (diameter)}} \times 100$$

3. Results and discussion

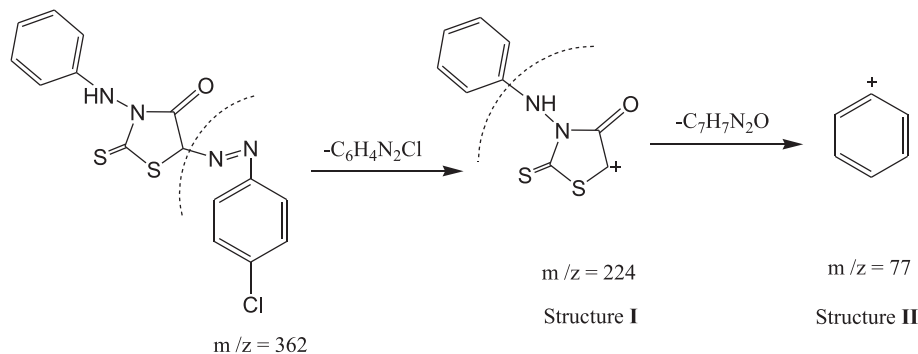
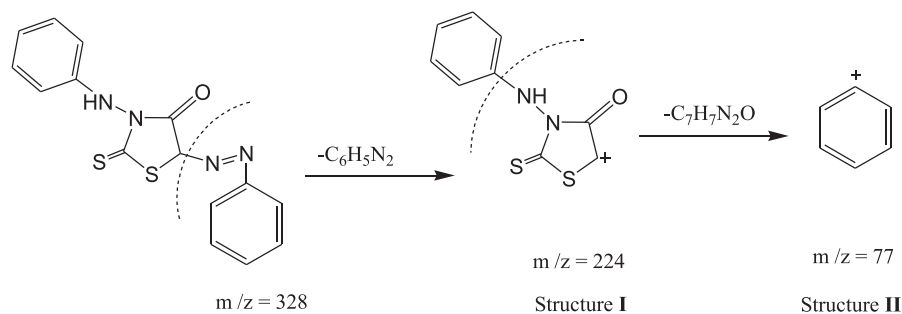
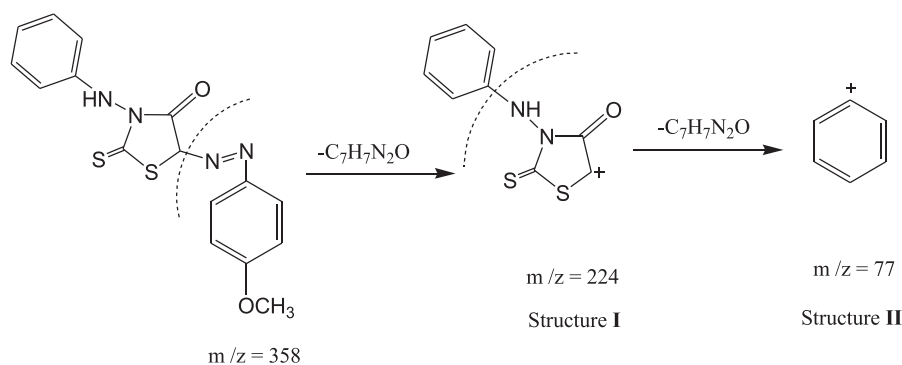
3.1. Molecular structure

The molecular structures of the ligands (**HL_n**) were optimized by HF method with 3-21G basis set. The molecules were built with the Perkin Elmer ChemBioDraw and optimized using Perkin Elmer ChemBio3D software. The geometrical parameters bond lengths and bond angles of **HL_n** are calculated and presented in Fig. 3 and Tables 2–6. Molecular

structures (HOMO & LUMO) for **HL_n** are presented in Fig. 4. The HOMO–LUMO energy gap, ΔE , which is an important stability index, is applied to develop theoretical models for explaining the structure and conformation barriers in many molecular systems. The smaller the value of ΔE is, the more the stability the compound has [3,18]. The calculated quantum chemical parameters are given in Table 7. Additional parameters such as separation energies, ΔE , absolute electronegativities, χ , chemical potentials, μ , absolute hardness, η , absolute softness, σ , global electrophilicity, ω [29], global softness, S , and additional electronic charge, ΔN_{max} , have been calculated according to the following Eqs. (2–9):

$$\Delta E = E_{\text{LUMO}} - E_{\text{HOMO}} \quad (2)$$

$$\chi = \frac{-(E_{\text{HOMO}} + E_{\text{LUMO}})}{2} \quad (3)$$



Scheme 1. a. Fragmentation patterns of **HL₁**, b. Fragmentation patterns of **HL₃**, c. Fragmentation patterns of **HL₄**.

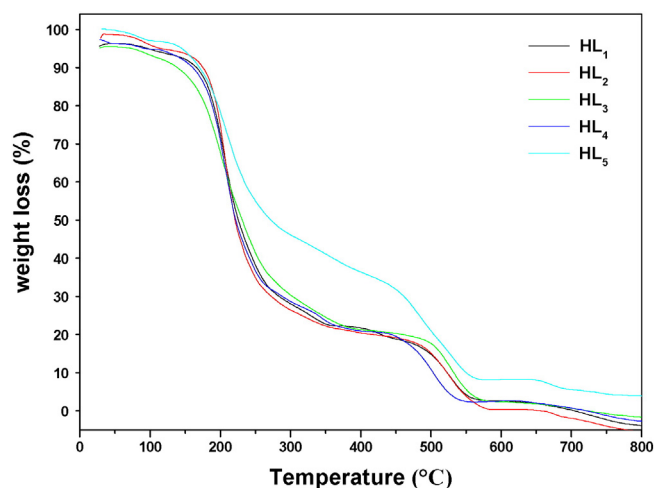


Fig. 8. TGA curves of ligands HL

$$\eta = \frac{E_{LUMO} - E_{HOMO}}{2} \quad (4)$$

$$\sigma = 1/\eta \quad (5)$$

$$Pi = -\chi \quad (6)$$

$$S = \frac{1}{2\eta} \quad (7)$$

$$\omega = Pi^2/2\eta \quad (8)$$

$$\Delta N_{max} = -Pi/\eta \quad (9)$$

The value of ΔE for ligands **HL₁**, **HL₂**, **HL₃**, **HL₄** and **HL₅** was found 1.338, 1.575, 1.703, 1.281 and 4.245 eV, respectively. The calculations indicated that the **HL₄** is more stable form than the other ligands [3]. The relation between Hammett's substitution coefficients (σ^R) vs. energy gap (ΔE) is shown in Fig. 5. It is clear that the values increase with increasing σ^R .

3.2. Metal complexes

The interaction of hydrazone ligands (**HL_n**) with $[\text{Co}(\text{CH}_3\text{COO})_2] \cdot 4\text{H}_2\text{O}$ in a molar ratio 2:3 [**Co**:**HL_n**] under reflux conditions gave the polymeric products presented in Table 1. The polymeric Co(II) complexes are stable in air and soluble in DMF and DMSO. The molar conductance values for the cobalt (II) complexes (10^{-3} M) are measured in DMF at 25 °C and

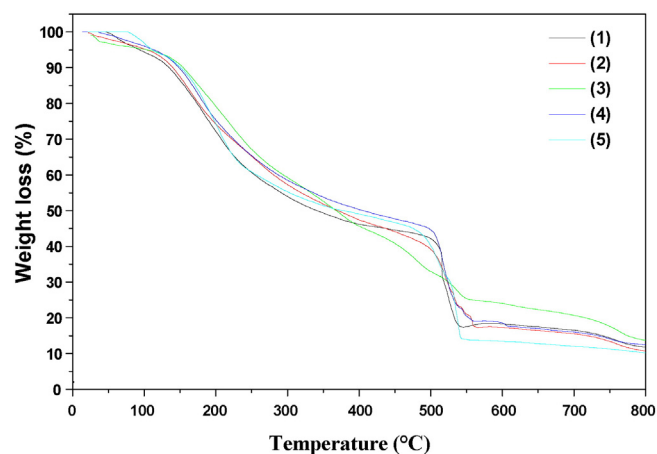


Fig. 9. TGA curves of complexes (1–5).

Table 10

Thermal analysis data of the complexes (1–5).

Complex ^a	Temp. range (°C)	Found mass loss (calc.) %	Assignment
(1)	0–140	11.4 (11.45)	Loss of C ₄ H ₁₀ O ₆ .
	140–510	50.49 (50.75)	Loss of C ₃₂ H ₂₆ N ₈ O ₂ S ₄ .
	510–800	26.41 (26.64)	Loss of C ₁₆ H ₁₄ N ₄ O ₂ S ₂ .
	>800	11.7 (11.15)	Loss of 2CoO
(2)	0–145	11.19 (11.88)	Loss of C ₄ H ₁₀ O ₆ .
	145–505	50.95 (50.15)	Loss of C ₃₂ H ₂₆ N ₈ S ₄ .
	505–800	25.9 (26.39)	Loss of C ₁₆ H ₁₄ N ₄ OS ₂ .
	>800	11.96 (11.56)	Loss of 2CoO
(3)	0–160	11.97 (12.27)	Loss of C ₄ H ₁₀ O ₆ .
	160–550	49.73 (49.6)	Loss of C ₃₀ H ₂₂ N ₈ S ₄ .
	550–800	25.8 (26.15)	Loss of C ₁₅ H ₁₂ N ₄ OS ₂ .
	>800	12.8 (11.95)	Loss of 2CoO
(4)	0–155	11.42 (11.34)	Loss of C ₄ H ₁₀ O ₆ .
	155–515	50.36 (50.9)	Loss of C ₃₀ H ₂₀ N ₈ S ₄ Cl ₂ .
	515–800	26.4 (26.7)	Loss of C ₁₅ H ₁₁ N ₄ OS ₂ Cl.
	>800	11.82 (11.04)	Loss of 2CoO
(5)	0–155	11.03 (11.08)	Loss of C ₄ H ₁₀ O ₆ .
	155–525	51.33 (51.26)	Loss of C ₃₀ H ₂₀ N ₁₀ O ₄ S ₄ .
	525–800	26.28 (26.85)	Loss of C ₁₅ H ₁₁ N ₅ O ₃ S ₂ .
	>800	10.36 (10.7)	Loss of 2CoO

^a Numbers as given in Table 1.

these values are in the range of 4–12 Ω⁻¹ cm² mol⁻¹ indicating a non-electrolytic nature [23]. The non-electrolytic nature of the Co(II) polymeric complexes implies the contribution of acetate ions to the coordination sphere in the complexes under investigation.

Table 9

Thermal analysis data of the ligands (**HL_n**).

Compound	Temp. range (°C)	Found mass loss (calc.) %	Assignment
HL₁	30–260	62 (61.9)	Decomposition of a part of the ligand (C ₉ H ₆ N ₂ S ₂ O).
	260–570	30 (29.6)	Further decomposition of a part of the ligand (C ₆ H ₆ N ₂).
	570–800	8 (8.6)	Further decomposition of a part of the ligand (OCH ₃).
HL₂	30–265	65 (64.9)	Decomposition of a part of the ligand (C ₉ H ₆ N ₂ S ₂ O).
	265–700	30 (30.9)	Further decomposition of a part of the ligand (C ₆ H ₆ N ₂).
	700–800	5 (4.3)	Further decomposition of a part of the ligand (CH ₃).
HL₃	30–330	68 (67.7)	Decomposition of a part of the ligand (C ₉ H ₆ N ₂ S ₂ O).
	330–800	32 (32.3)	Further decomposition of a part of the ligand (C ₆ H ₆ N ₂).
	30–350	71 (71.3)	Decomposition of a part of the ligand (C ₉ H ₇ N ₂ S ₂ OCl).
HL₄	350–800	29 (28.9)	Further decomposition of a part of the ligand (C ₆ H ₅ N ₂).
	30–400	59 (59.5)	Decomposition of a part of the ligand (C ₉ H ₆ N ₂ S ₂ O).
	400–600	28 (28.4)	Further decomposition of a part of the ligand (C ₆ H ₆ N ₂).
HL₅	600–800	13 (12.3)	Further decomposition of a part of the ligand (NO ₂).

Evidence for all polymeric nature comes from its solubility properties and the metal polymer complex to ligand stoichiometry which is shown to be 2:3 from the elemental analysis. IR spectroscopy provides partial evidence that the ligand is acting as a bridge, and that bridging occurs through both the S and NH from side and through O and N (hydrazone) from the other side.

3.3. Infrared spectra and nature of coordination

The three bands around 823–882, 3205–3210 and 1727–1754 cm^{-1} in the ligands assigned to $\nu(\text{CS})$, $-\text{NH}(3\text{-phenylamine})$ and $\nu(\text{CO})$ groups, respectively, were shifted to lower frequencies and $-\text{NH}(3\text{-phenylamine})$ disappearance in all polymer complexes. This indicates

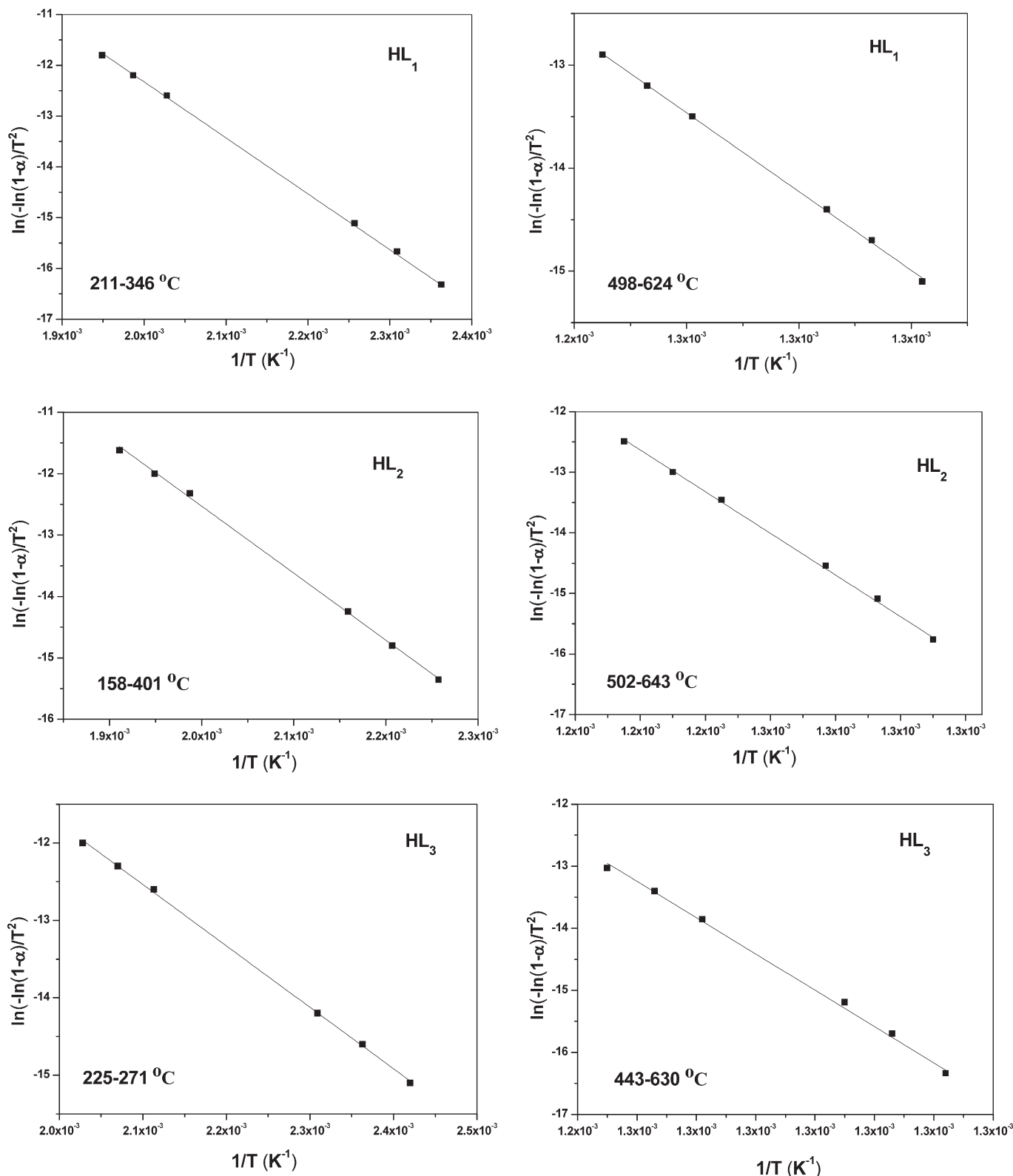


Fig. 10. Coats-Redfern (CR) of ligands (HL_n), Stages (I, II).

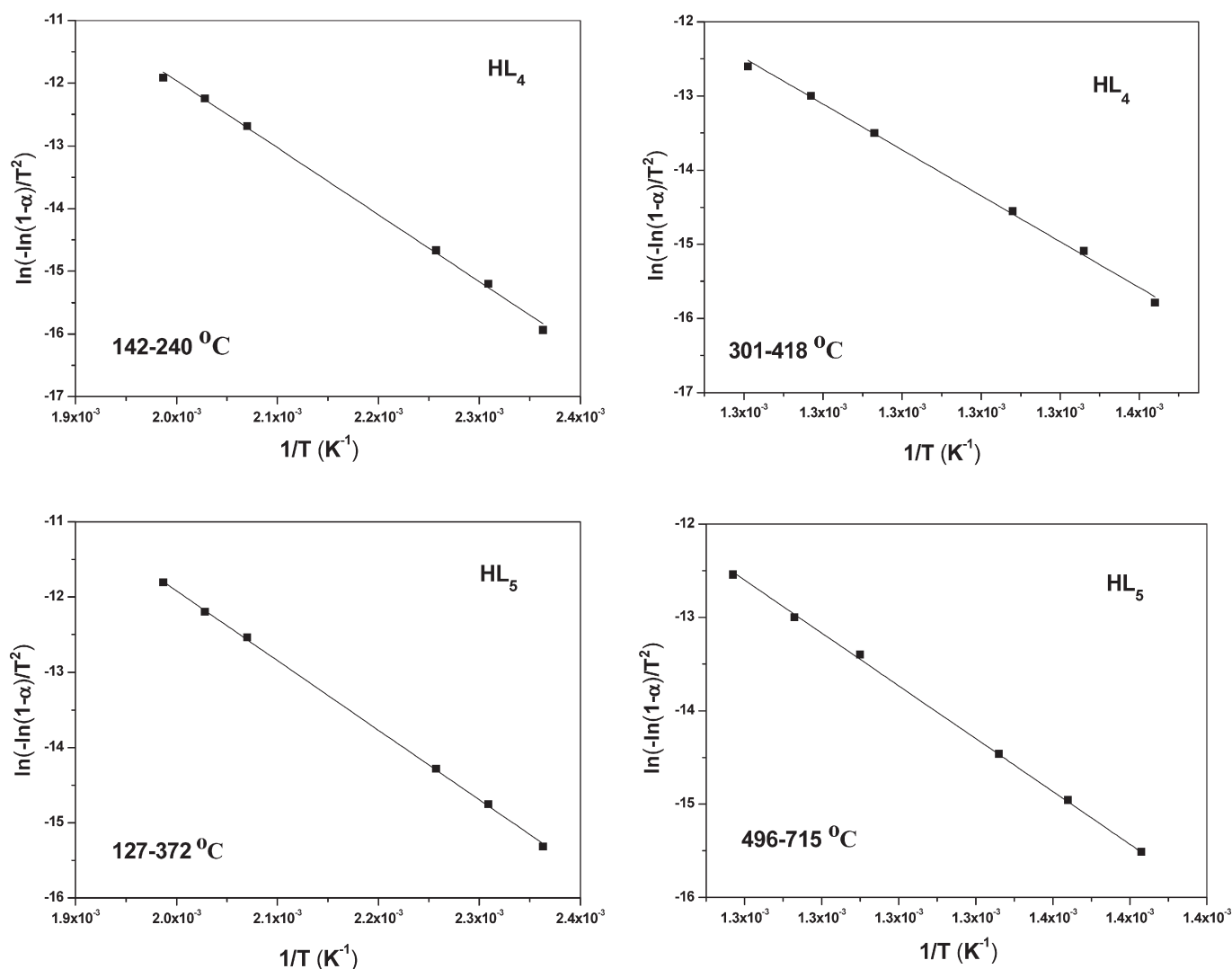


Fig. 10 (continued).

the participation of the thione sulfur, NH(3-phenylamine) and carbonyl oxygen groups, in the chelation (Table 8) [30]. The splitting of $\nu(\text{N}=\text{N})$ band into two bands in the ranges 1435–1520 and ~ 1230 cm⁻¹ due to $\nu(\text{HC}=\text{N})$ and $\nu(\text{N}=\text{NH})$ hydrazone, respectively, for ligands provides an evidence that the hydrazone N participate in the chelation after deprotonation leading to a covalent linkage. This is more rather confirmed from the observation of Karabatoses et al. [31] and El-Sonbati et al. [32] where the hydrazone form is more than the azo structure for similar compounds (Fig. 1D). In all polymer complexes, CN group remained intact, indicating the non-participation of the azomethine nitrogen in the chelation [33]. The strong observed at ~ 1111 – 1123 cm⁻¹ may be assigned to $\nu(\text{N}-\text{N})$ vibration mode [34] is affected on complexation. It is blue shifted and appearance as a weak band. In all polymer complexes, there are two bands ν_{as} (1427–1444) and ν_{s} (1230–1243) cm⁻¹ stretching vibration of acetate group. The correlation between the positions of the antisymmetric and symmetric stretching vibration of this group was earlier studied [35]. It was concluded from these studies that the frequency difference between the two carbonyl stretches of ionic acetate groups is usually in the interval ~ 160 cm⁻¹, longer values were found for monodentate and lower values for bidentate groups [36]. Correspondingly, the split of 195–201 cm⁻¹ in polymer complexes indicates monodentate acetate. This is supported by results of Ryde [37].

The above interpretation is further supported by the appearance of the non-ligand bands at: 680–690 cm⁻¹; $\nu(\text{Co}-\text{O})$, 528–598 cm⁻¹; $\nu(\text{Co}-\text{N})$ [38] and 480–500 cm⁻¹; $\nu(\text{Co}-\text{S})$ [39]. Such class of compounds is with different types of hydrogen bonding [2–6]:

1. H-bonding of the type $\text{NH}\cdots\text{O}$ between the $-\text{NH}$ (hydrazone) group and $\text{C}=\text{O}$ group.
2. Intermolecular hydrogen bonding of the $\text{NH}\cdots\text{O}$ type of one molecule to another one.
3. The case is more favored. This is due to the presence of a broad band located at 870–965 cm⁻¹ which could be taken as a good evidence for the intermolecular hydrogen bonding.

In all polymer complexes ~ 3500 – 3200 cm⁻¹ is observed, such region is attributed to different probabilities: (i) it is due to either free OH or NH, (ii) bonded $-\text{OH}$ group or $-\text{NH}$ group or (iii) due to the presence of coordinated water molecules.

3.4. ¹H NMR spectra

The ¹H NMR spectra of the ligands are recorded in dimethylsulfoxide (DMSO-d₆) solution using tetramethylsilane (TMS) as internal standard. The broad signal exhibited by the ligands can be assigned to

intramolecular hydrogen bonded proton of NH (hydrazone) at ~11.5 ppm and NH(3-phenylamine) at ~9.0 ppm were not affected by dilution and disappear in the presence of D₂O. The chemical shifts of the different types of protons in the ¹H NMR spectra of the ligands

(HL₁ and HL₂) display sharp signals at 3.7 and 2.3 ppm with an integration equivalent to three hydrogens corresponding to the O-CH₃ and C-CH₃ groups, respectively. The aromatic rings give a group of multi signals at 6.5–8.0 ppm.

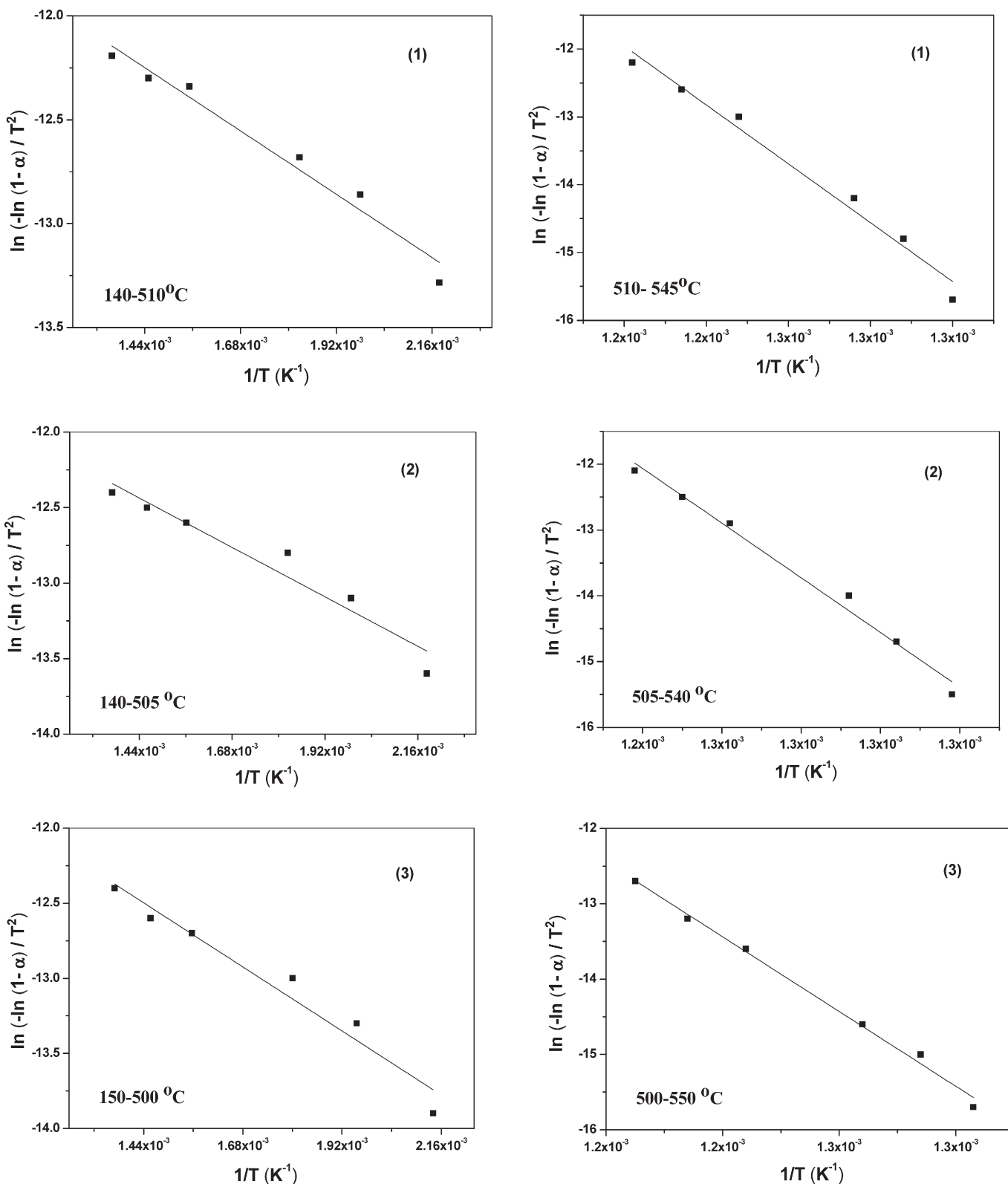


Fig. 11. Coats–Redfern (CR) of Co(II) complexes (1–5), Stages (I, II).

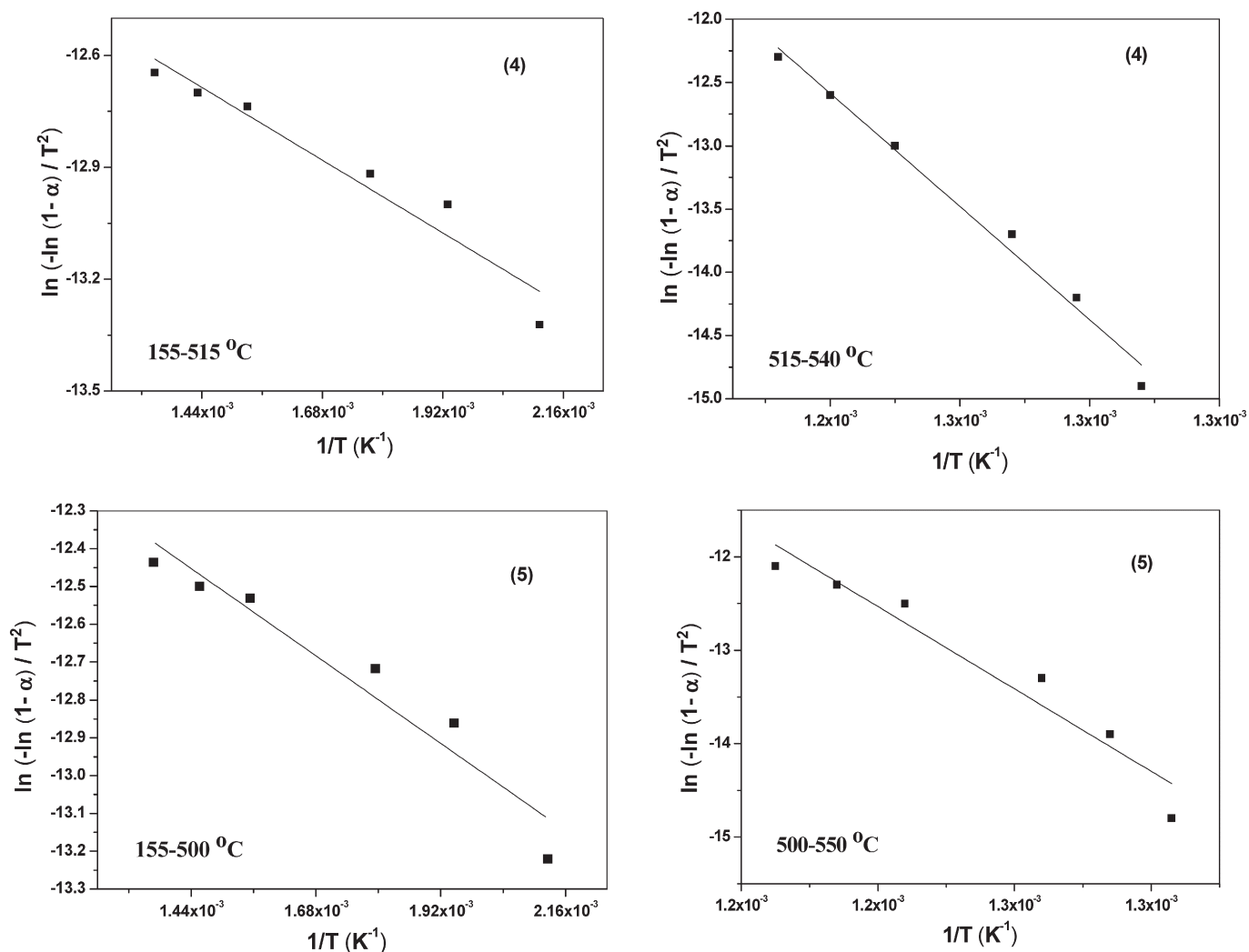


Fig. 11 (continued).

The ¹³C NMR of ligands exhibited signals at 170–172 ppm corresponding to the carbon of (C=N) groups, signals appear at 160–163 ppm corresponding to (C=O) groups and signals around ~200 ppm corresponding to the carbon of (C=S). Ligands have different chemical shift due to aromatic ring substituent. Therefore, it is clear from these results that the data obtained from the elemental analyses; IR and ¹H NMR spectra measurements are in agreement with each other.

3.5. X-ray diffraction analysis

The X-ray diffraction (XRD) patterns of **HL₁**, **HL₃** and **HL₄** ligands and complex (**1**) in powder forms are shown in Fig. 6. The XRD patterns of **HL₁**, **HL₃** and **HL₄** ligands show many sharp diffraction peaks in addition to a broad hump at $2\theta = 8^\circ$. This behavior indicates that the powder is a mixture of amorphous and polycrystalline nature. The XRD pattern of complex (**1**) shows amorphous nature.

3.6. Mass spectra

The mass spectra of ligands (**HL₁**, **HL₃** and **HL₄**) are recorded and investigated at 70 eV of electron energy. It is obvious that, the molecular ion peaks are in good agreement with their suggested empirical formula as indicated from elemental analyses (Table 1). The mass spectrum

fragmentation mode of ligand (**HL₁**) shows the exact mass of 358 corresponding to the formula C₁₆H₁₄N₄O₂S₂ (Fig. 7a). The ion of $m/z = 358$ undergoes fragmentation to a stable peak at $m/z = 224$ by losing C₇H₇N₂O atoms (structure I) as shown in Scheme (1a). A breakdown of the backbone of **HL₁** ligand gives the fragment (structure II) with $m/z = 77$ by losing of C₃H₂N₂OS₂.

The mass spectrum fragmentation mode of ligand (**HL₃**) shows the exact mass of 328 corresponding to the formula C₁₅H₁₂N₄OS₂ (Fig. 7b). The ion of $m/z = 328$ undergoes fragmentation to a stable peak at $m/z = 224$ by losing C₆H₅N₂ atoms (structure I) as shown in Scheme (1b). A breakdown of the backbone of **HL₃** ligand gives the fragment (structure II) with $m/z = 77$ by losing of C₃H₂N₂OS₂.

The mass spectrum fragmentation mode of ligand (**HL₄**) shows the exact mass of 362.5 corresponding to the formula C₁₅H₁₁N₄OS₂Cl (Fig. 7c). The ion of $m/z = 362$ undergoes fragmentation to a stable peak at $m/z = 224$ by losing C₆H₄N₂Cl atoms (structure I) as shown in Scheme (1c). A breakdown of the backbone of **HL₄** ligand gives the fragment (structure II) with $m/z = 77$ by losing of C₃H₂N₂OS₂.

3.7. Electronic spectra and magnetic measurements

The electronic absorption spectra of the two ligands (**HL_n**) exhibits bands at 26,350–26,150 cm⁻¹ (CS) ($n \rightarrow \pi^*$), 30,460–30,250 cm⁻¹ (CO) ($n \rightarrow \pi^*$), 32,980–33,100 cm⁻¹ (H-bonding and association),

40,240–39,890 cm^{-1} (phenyl) (ph-ph^* , $\pi-\pi^*$) [40] and 29,610–29,350 cm^{-1} transition of phenyl rings overlapped by composite broad $\pi-\pi^*$ of azo/ $\text{CH}=\text{N}$ structure. In the Co(II) complexes, the (CS and CO) ($n-\pi^*$) transition shifts to lower energy. These shifts or the

disappearance of the bands are indicative of coordination of the ligands are indicative of coordination of the ligands to Co(II) .

Based on magnetic moment values, the cobalt(II) compounds fall into two classes. In the first, the so called ionic complexes are with μ_{eff}

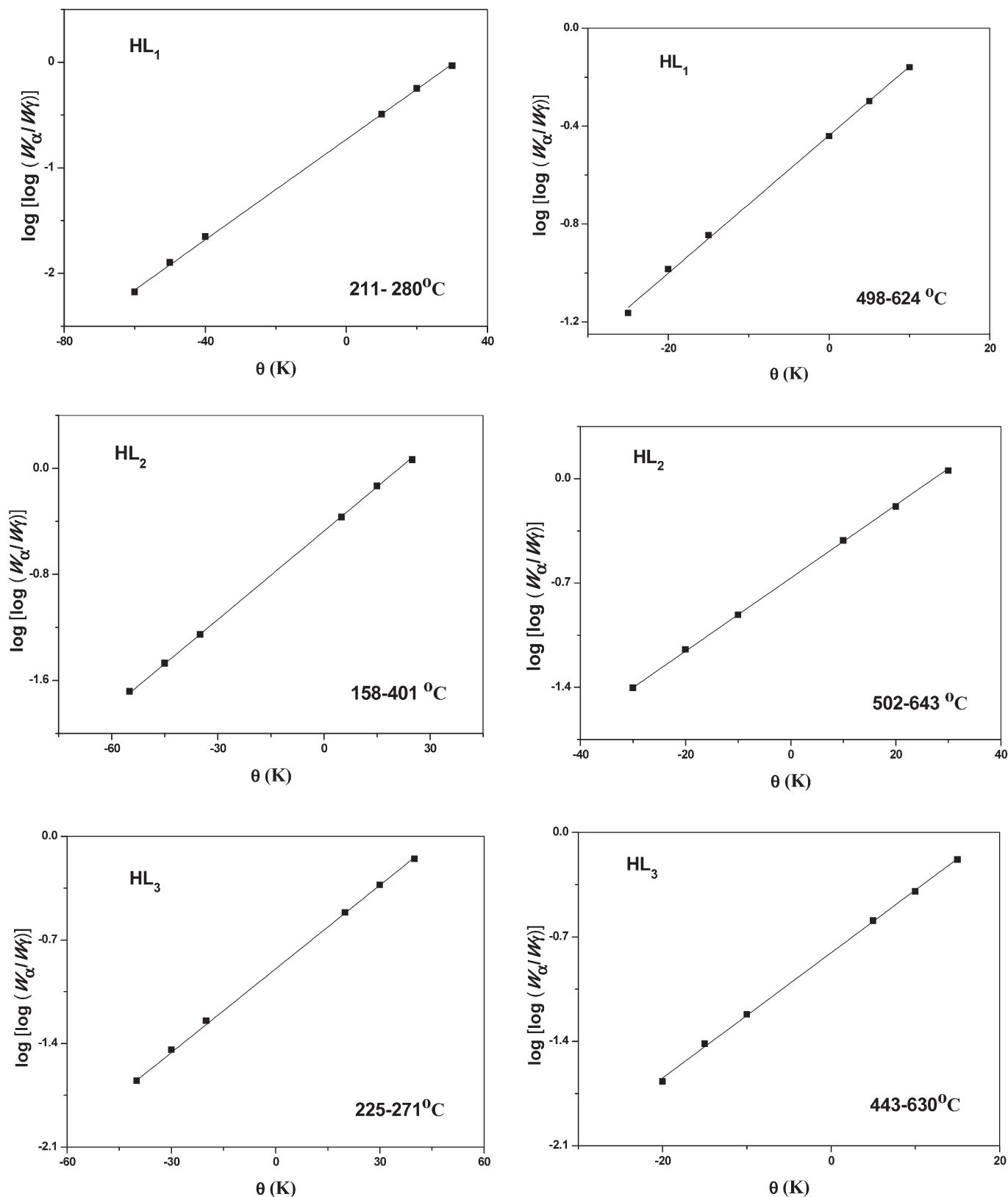


Fig. 12. Horowitz–Metzger (HM) of ligands (HL_n), stages (I, II).

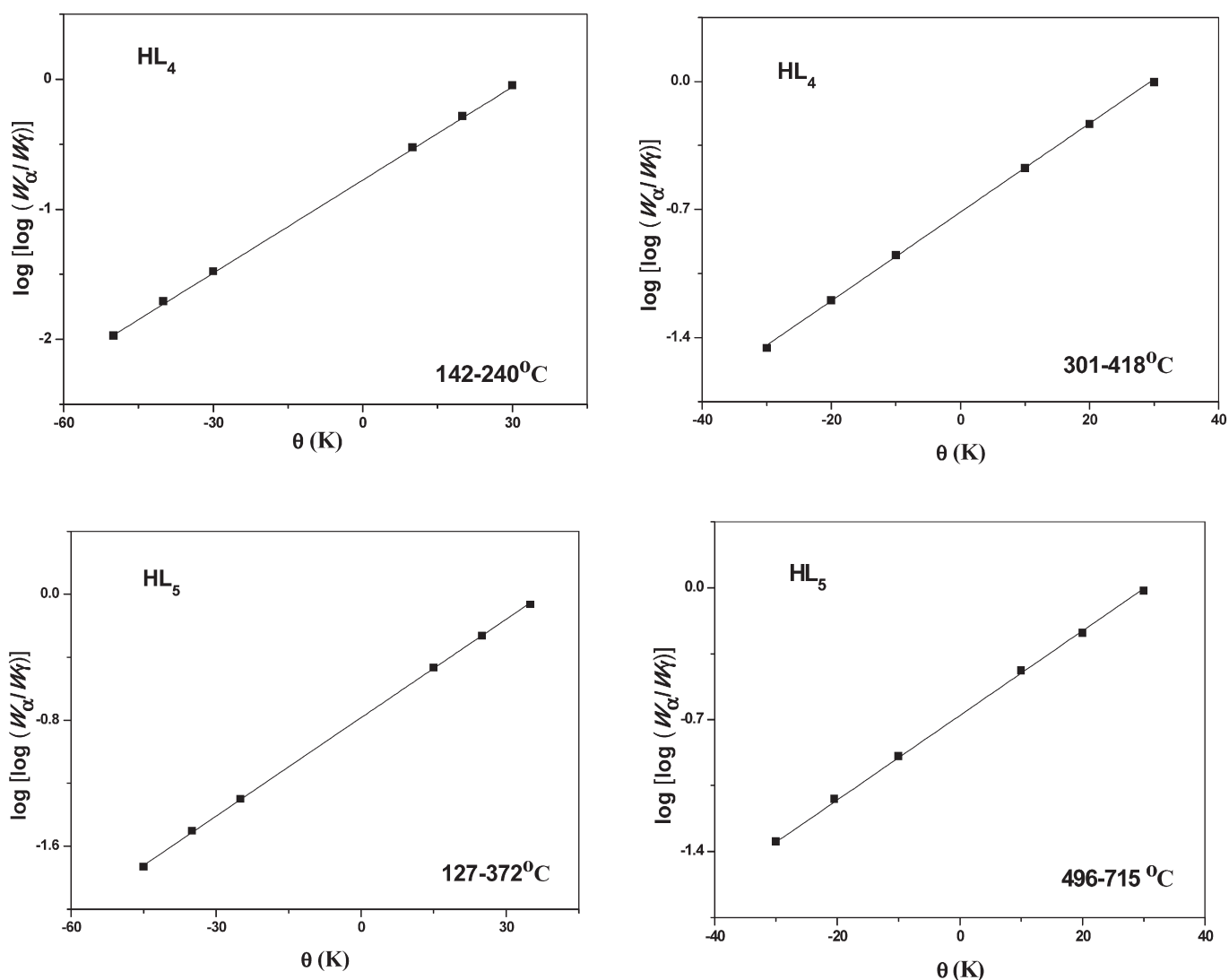


Fig. 12 (continued).

values lying in the first range 4.3–5.6 B.M., while the second is with much smaller values (1.7–2.9 B.M.) and are of covalent properties. From such scope of representation, the first class of cobalt(II) complexes. (i) may be associated with low spin octahedral field, while the second class (ii) is of square planar environment around cobalt(II). The spectra of our data exhibited bands located at 9200–2210 and 43,320–4400 cm^{-1} . Such finding is a strong indicative of octahedral spatial configuration. It is of interest to mention that the low magnetic moments of Co(II) complexes ($\mu_{\text{eff.}} = 1.15\text{--}1.24$ B.M./atom) could be referred to occur through a ligand bridge as shown in Fig. 2. Another reason for the lowering magnetic moments may be due to the admixture of cobalt(II) and cobalt(III) ions in the same molecule.

3.8. Thermal analysis

The TGA curves for the ligands (HL_n) are shown in Fig. 8. It is clear that the change of substituent affects the thermal properties of the ligands. The temperature intervals and the percentage of loss of masses are listed in Table 9.

HL_1 ligand shows three decomposition steps, the first stage that occurs in the temperature range 30–260 °C is attributed to loss of $C_9H_6N_2S_2O$ (found 62.0% and calc. 61.9%). The second stage in the temperature range 260–570 °C corresponds to loss of a part of the ligand

($C_6H_6N_2$) (Found 30.0%, calc. 29.6%). The third stage in the temperature range 570–800 °C corresponds to loss of a part of the ligand (OCH_3) (Found 8.0%, calc. 8.6%).

HL_2 ligand shows three decomposition steps, the first stage that occurs in the temperature range 30–265 °C is attributed to loss of ($C_9H_6N_2S_2O$) (found 65.0% and calc. 64.9%). The second stage in the temperature range 265–700 °C corresponds to loss of a part of the ligand ($C_6H_6N_2$) (found 30.0%, calc. 30.9%). The third stage in the temperature range 700–800 °C corresponds to loss of a part of the ligand (CH_3) (Found 5.0%, calc. 4.3%).

HL_3 ligand shows two decomposition steps, the first stage that occurs in the temperature range 30–330 °C is attributed to loss of ($C_9H_6N_2S_2O$) (found 68.0% and calc. 67.7%). The second stage in the temperature range 330–800 °C corresponds to loss of a part of the ligand ($C_6H_5N_2$) (found 32.0%, calc. 32.3%).

HL_4 ligand shows two decomposition steps, the first stage that occurs in the temperature range 30–350 °C is attributed to Loss of ($C_9H_7N_2S_2OCl$) (found 71.0% and calc. 71.3%). The second stage in the temperature range 350–800 °C corresponds to loss of a part of the ligand ($C_6H_5N_2$) (found 29.0%, calc. 28.9%).

HL_5 ligand shows three decomposition steps, the first stage that occurs in the temperature range 30–400 °C is attributed to Loss of ($C_9H_6N_2S_2O$) (found 59.0% and calc. 59.5%). The second stage in the

temperature range 400–600 °C corresponds to loss of a part of the ligand ($C_6H_6N_2$) (found 28.0%, calc. 28.4%). The third stage in the temperature range 700–800 °C corresponds to loss of a part of the ligand (NO_2) (found 13.0%, calc. 12.3%).

The TGA curves for Co(II) complexes (1–5) are shown in Fig. 9. The temperature intervals and the percentage of loss of masses are listed in Table 10. The TG curves of all Co (II) complexes (1–5) showed the loss of $C_4H_{10}O_6$ in the temperature range ~30–150 °C. The first stage is

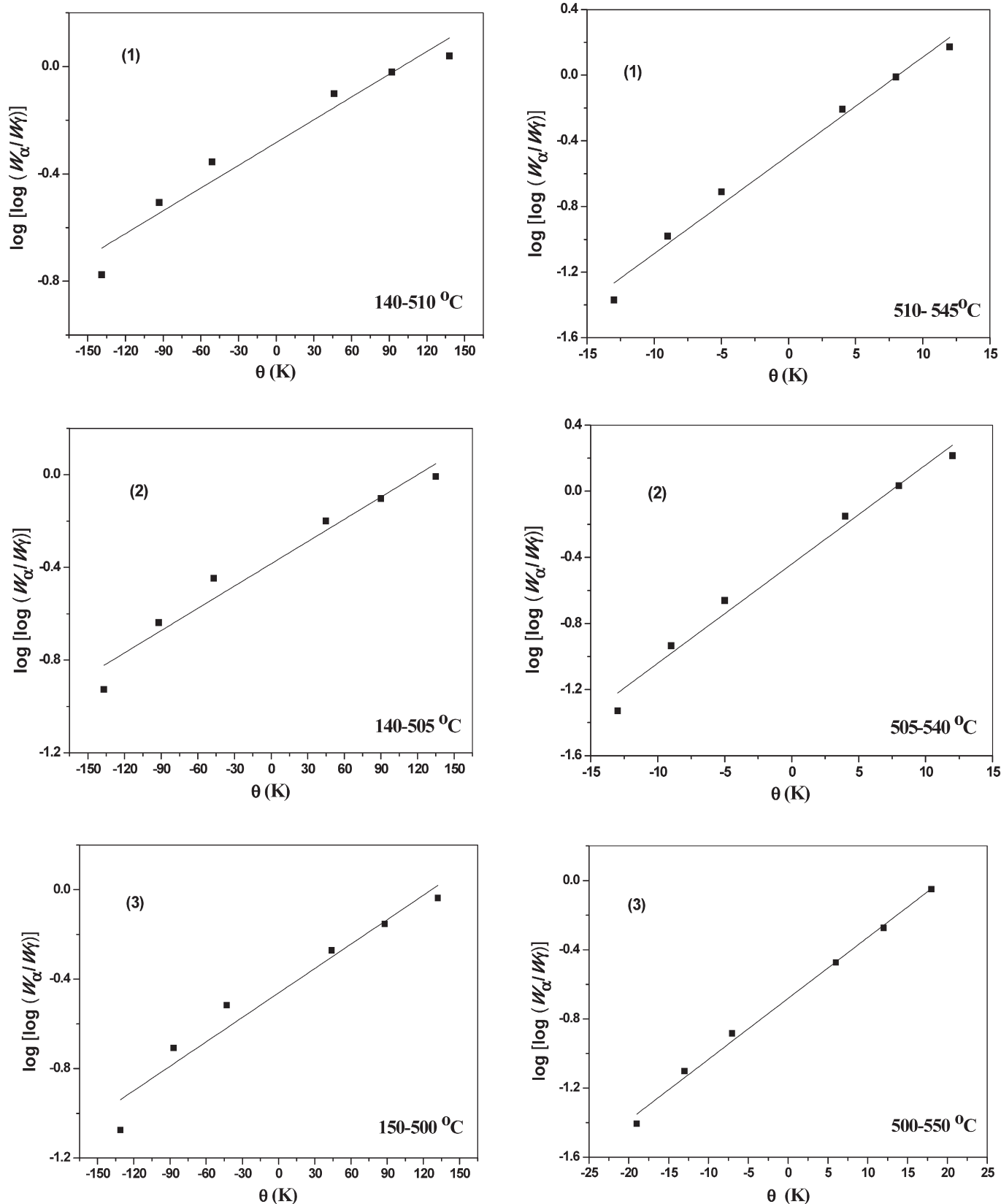


Fig. 13. Horowitz–Metzger (HM) of Co(II) complexes (1–5), stages (I, II).

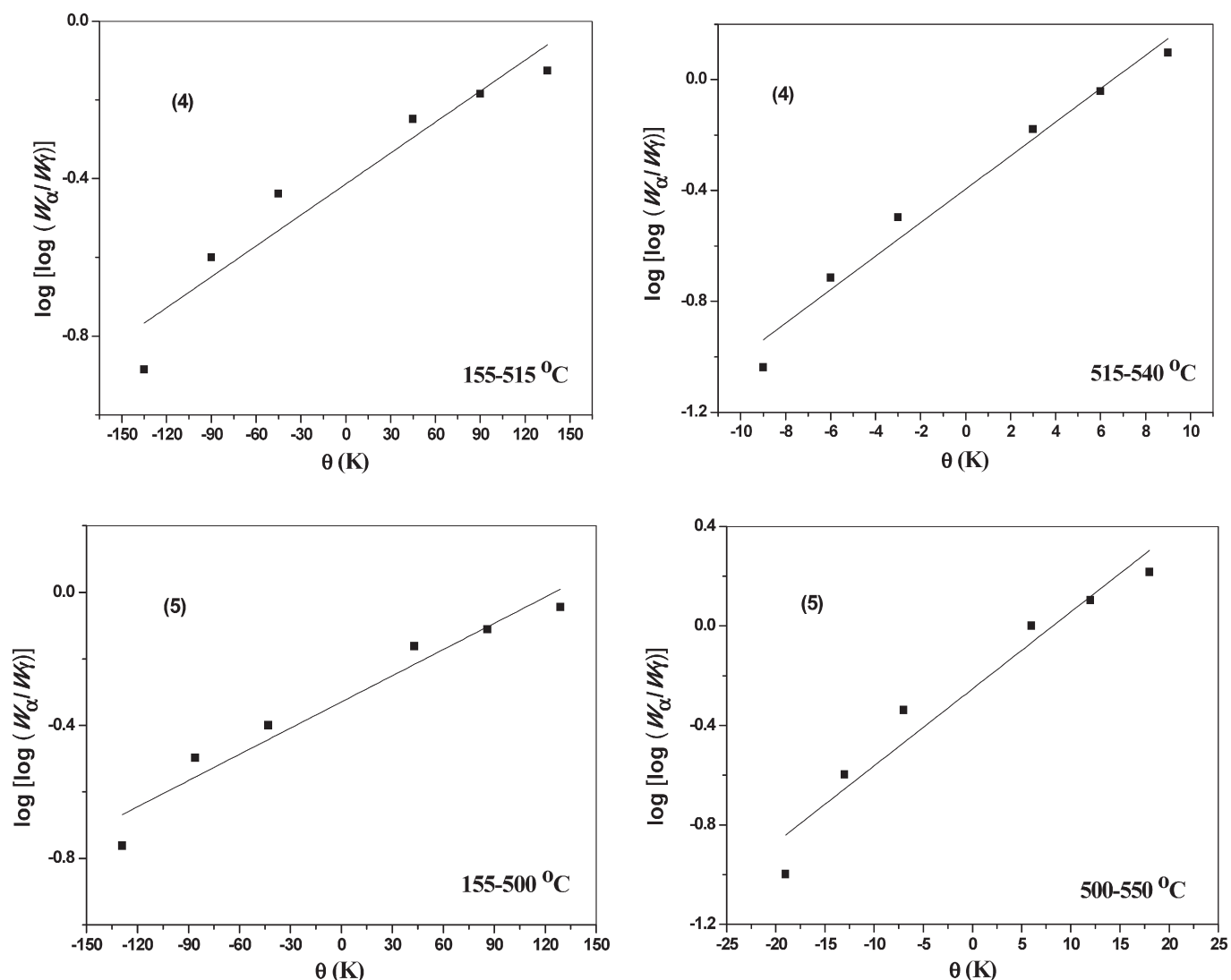


Fig. 13 (continued).

Table 11

Thermodynamic data of the thermal decomposition of ligands (HL_n).

Compound	Decomposition temperature (°C)	Method	Parameter					R
			E _a (kJ mol ⁻¹)	A (s ⁻¹)	ΔS [*] (J mol ⁻¹ K ⁻¹)	ΔH [*] (kJ mol ⁻¹)	ΔG [*] (kJ mol ⁻¹)	
HL ₁	211–346	CR	45.8	7.58 × 10 ¹	–214	41.2	159	0.99221
		HM	53.6	4.18 × 10 ²	–200	49	159	0.99398
	498–624	CR	180	4.43 × 10 ⁸	–87.9	174	247	0.99355
		HM	193	6.40 × 10 ⁹	–65.8	186	241	0.99169
HL ₂	158–401	CR	46.9	7.11 × 10 ¹	–215	42.3	161	0.99322
		HM	48.4	1.17 × 10 ²	–210	43.8	160	0.99788
	502–643	CR	162	2.34 × 10 ⁷	–113	155	250	0.98442
		HM	173	2.50 × 10 ⁸	–92.2	166	245	0.99156
HL ₃	225–271	CR	329	2.54 × 10 ³⁰	333	325	151	0.99453
		HM	338	1.70 × 10 ³²	367	333	142	0.99452
	443–630	CR	108	1.51 × 10 ⁴	–173	101	242	0.99432
		HM	120	2.05 × 10 ⁵	–152	113	236	0.9939
HL ₄	142–240	CR	70.9	5.53 × 10 ⁵	–139	67.1	131	0.99122
		HM	80.8	1.40 × 10 ⁷	–112	76.9	129	0.98595
	301–418	CR	102	1.31 × 10 ⁶	–134	96.5	181	0.99104
		HM	114	2.10 × 10 ⁷	–111	108	179	0.99064
HL ₅	127–372	CR	31.2	3.31 × 10 ⁰	–240	26.9	152	0.99523
		HM	39.2	3.59 × 10 ¹	–220	34.9	150	0.98744
	496–715	CR	108	1.59 × 10 ⁴	–173	101	254	0.98712
		HM	119	5.78 × 10 ⁴	–163	112	255	0.98669

Table 12
Thermodynamic data of the thermal decomposition of Co(II) complexes (1–5).

Compound ^a	Decomposition temperature (°C)	Method	Parameter					R
			E _a (kJ mol ⁻¹)	A (s ⁻¹)	ΔS* (J mol ⁻¹ K ⁻¹)	ΔH* (kJ mol ⁻¹)	ΔG* (kJ mol ⁻¹)	
(1)	140–510	CR	10.6	6.31 × 10 ³	-293	5.59	181	0.96357
		HM	19.4	5.36 × 10 ²	-275	14.4	179	0.94125
	510–545	CR	722	2.20 × 10 ⁴⁵	615	715	223	0.97664
		HM	734	1.88 × 10 ⁴⁶	633	727	221	0.99571
(2)	140–505	CR	11.4	6.47 × 10 ³	-293	6.41	181	0.9262
		HM	21.7	9.87 × 10 ²	-270	16.8	177	0.9493
	505–540	CR	691	4.44 × 10 ⁴³	583	684	221	0.98464
		HM	726	1.14 × 10 ⁴⁶	629	719	220	0.98183
(3)	150–500	CR	14.8	1.43 × 10 ²	-286	9.81	181	0.9478
		HM	25	2.14 × 10 ¹	-264	20	178	0.93629
	500–550	CR	412	6.11 × 10 ²⁴	221	406	229	0.99286
		HM	430	1.77 × 10 ²⁶	249	423	224	0.99395
(4)	155–515	CR	6.76	1.35 × 10 ³	-306	1.70	188	0.92499
		HM	18.6	3.95 × 10 ²	-278	13.5	182	0.90661
	515–540	CR	744	8.17 × 10 ⁴⁶	645	738	221	0.98471
		HM	740	5.05 × 10 ⁴⁶	641	734	221	0.97099
(5)	155–500	CR	8	2.51 × 10 ³	-301	3.01	183	0.9166
		HM	18.1	3.83 × 10 ²	-278	13.1	180	0.93422
	500–550	CR	367	1.50 × 10 ²²	171	360	223	0.92419
		HM	377	5.83 × 10 ²²	183	371	225	0.93396

^a Numbers as given in Table 1.

related to loss of the part of the deprotonated ligand. The second stage is related to loss of **HL_n**. The final weight losses are due to the decomposition of metal oxides residue (Table 10).

3.8.1. Calculation of activation thermodynamic parameters

The thermodynamic activation parameters of decomposition processes of the ligands **HL_n** and their Co(II) complexes (1–5) namely activation energy (E_a), enthalpy (ΔH*), entropy (ΔS*), and Gibbs free energy change of the decomposition (ΔG*) are evaluated graphically by employing the Coats–Redfern [41] and Horowitz–Metzger [42] methods.

3.8.1.1. Coats–Redfern equation. The Coats–Redfern equation, which is a typical integral method, can represent as:

$$\int_0^\alpha \frac{dx}{(1-\alpha)^n} = \frac{A}{\phi} \int_{T_1}^{T_2} \exp\left(-\frac{E_a}{RT}\right) dt \quad (10)$$

For convenience of integration, the lower limit T₁ is usually taken as zero. This equation on integration gives

$$\ln\left[-\frac{\ln(1-\alpha)}{T^2}\right] = -\frac{E_a}{RT} + \ln\left[\frac{AR}{\phi E_a}\right] \quad (11)$$

A plot of left-hand side (LHS) against 1/T was drawn (Figs. 10 and 11). E_a is the energy of activation and calculated from the slope and A in (s⁻¹) from the intercept value. The entropy of activation (ΔS*) in (Jmol⁻¹ K⁻¹) is calculated by using the equation:

$$\Delta S^* = 2.303 \left[\log\left(\frac{Ah}{k_B T_s}\right) \right] R \quad (12)$$

Where k_B is the Boltzmann constant, h is the Plank's constant and T_s is the TG peak temperature.

3.8.1.2. Horowitz–Metzger equation. The Horowitz–Metzger equation is an illustrative of the approximation methods. These authors derived the relation:

$$\log\left[\frac{1-(1-\alpha)^{1-n}}{1-n}\right] = \frac{E_a \theta}{2.303 RT_s^2}, \text{ for } n \neq 1 \quad (13)$$

when n = 1, the LHS of Eq. (13) would be log[-log(1-α)] (Figs. 12 and 13). For a first order kinetic process, the Horowitz–Metzger equation may write in the form:

$$\log\left[\log\left(\frac{W_\alpha}{W_\gamma}\right)\right] = \frac{E_a \theta}{2.303 RT_s^2} - \log 2.303 \quad (14)$$

where θ = T - T_s, w_γ = w_α - w, w_α = mass loss at the completion reaction; w = mass loss up to time t. The plot of log [log (w_α/w_γ)] vs. θ was drawn and found to be linear from the slope of which E_a was calculated. The pre-exponential factor, A, is calculated from equation:

$$\frac{E_a}{RT_s^2} = \frac{A}{\left[\phi \exp\left(-\frac{E_a}{RT_s}\right)\right]} \quad (15)$$

The entropy of activation, ΔS*, is calculated from Eq. (12). The enthalpy activation, ΔH*, and Gibbs free energy, ΔG*, is calculated from:

$$\Delta H^* = E_a - RT \quad (16)$$

$$\Delta G^* = \Delta H^* - T\Delta S^* \quad (17)$$

The calculated values of E_a, A, ΔS*, ΔH* and ΔG* for the decomposition steps for ligands (**HL_n**) and cobalt(II) complexes (1–5) are summarized in Tables 11 and 12.

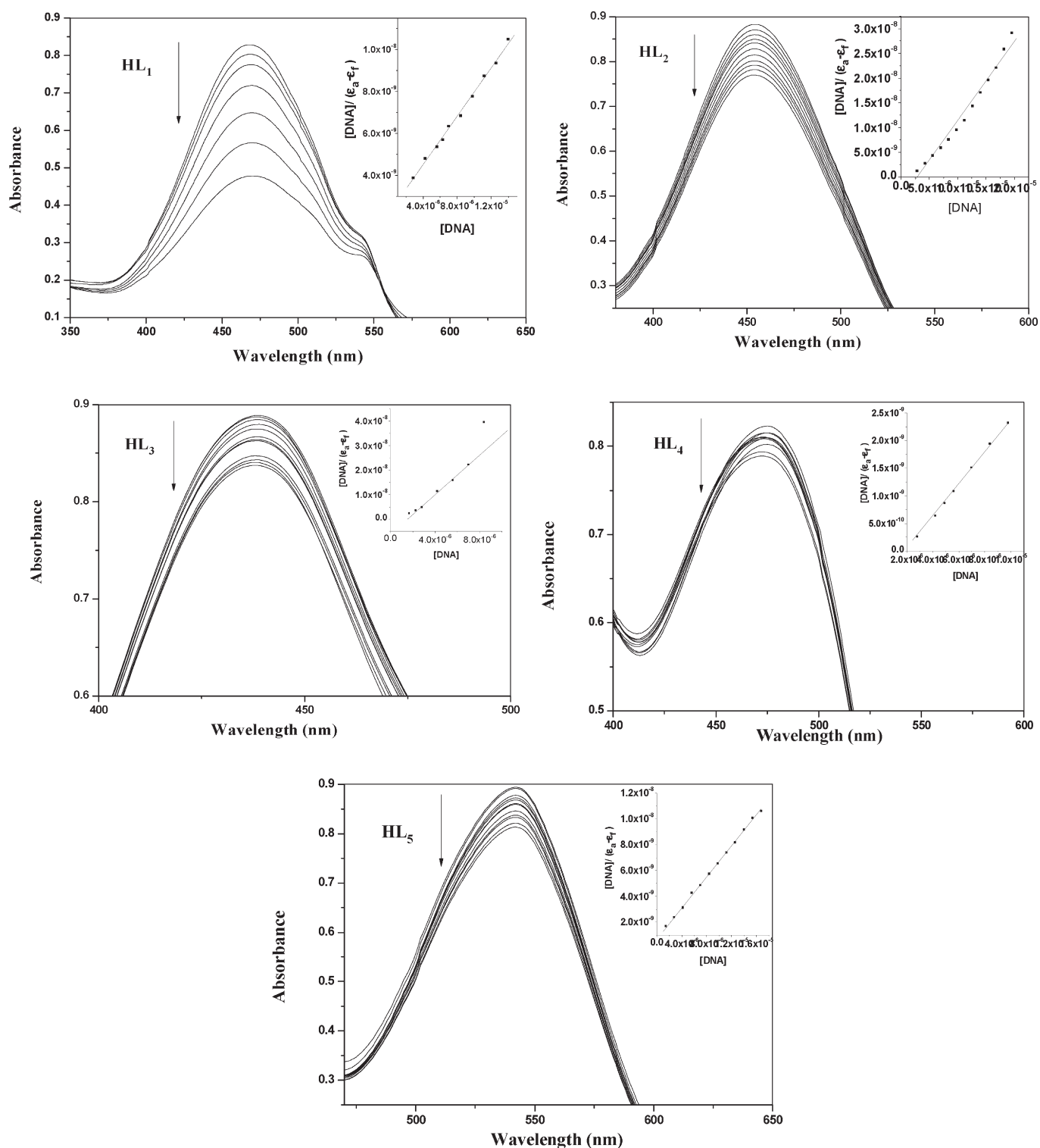


Fig. 14. Absorption spectra of ligands (**HL_n**) in buffer pH 7.2 at 25 °C in the presence of increasing amount of SS-DNA. Arrows indicate the changes in absorbance upon increasing the SS-DNA concentration. Inset: plot of $[DNA]/(\epsilon_a - \epsilon_f) \text{ M}^2 \text{ cm}$ vs. $[DNA] \text{ M}$ for titration of DNA with ligands (**HL_n**).

3.9. Stoichiometries of the cobalt(II) complexes

Analytical data of the polymeric complexes (Table 1) were isolated in the general formulae $[(\text{Co})_2(\text{L}_n)_2(\text{HL}_n)(\text{CH}_3\text{COO})_2(\text{OH}_2)_2]_n$ as shown in Fig. 2. The 2:3 stoichiometries of the polymeric complexes were calculated from their elemental analyses. The analytical data and the molar conductance measurements of the polymeric

complexes reveal that three molecules of the ligand and two of the anions are coordinated to the two metal atoms in all complexes. The ligands present four donor sites: the azo nitrogen, the carbonyl oxygen and the thionyl sulfur of rhodanine moiety and the NH group of 3-phenylamino. However, it is clear that the utilization of all the four bonding sites would introduce certain steric restrictions and hence either both the azo nitrogen and the carbonyl group

inhibitory concentration 50 (IC₅₀) was calculated from Fig. 16 and Table 13. The results clearly revealed that most of the compounds possessed cytotoxic activity as evidenced by the IC₅₀ values, as reported in Table 14. The results revealed that some tested compounds have

cytotoxic activity against the hepatocellular carcinoma (HePG-2) and mammary gland breast cancer (MCF-7) cell lines with superiority of HL₃ (IC₅₀ = 5.4 μg/mL and 5.6 μg/mL, respectively). All ligands HL_n exhibit highly significant cytotoxic activity against HePG-2 cell line.

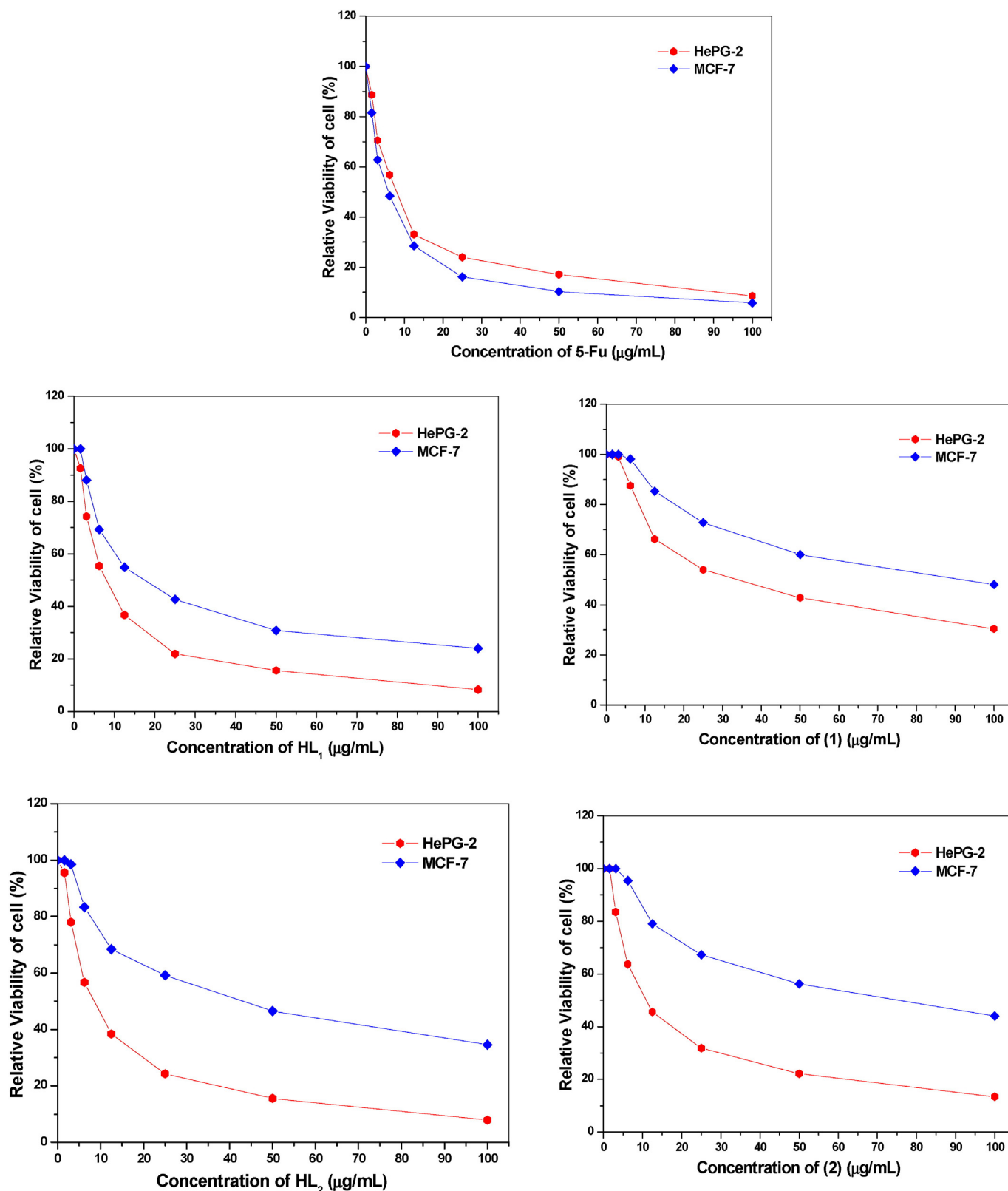


Fig. 16. Cytotoxic and antitumor activity of ligands (HL_n) and their Co(II) complexes (1–5) against HePG-2 and MCF-7 cells.

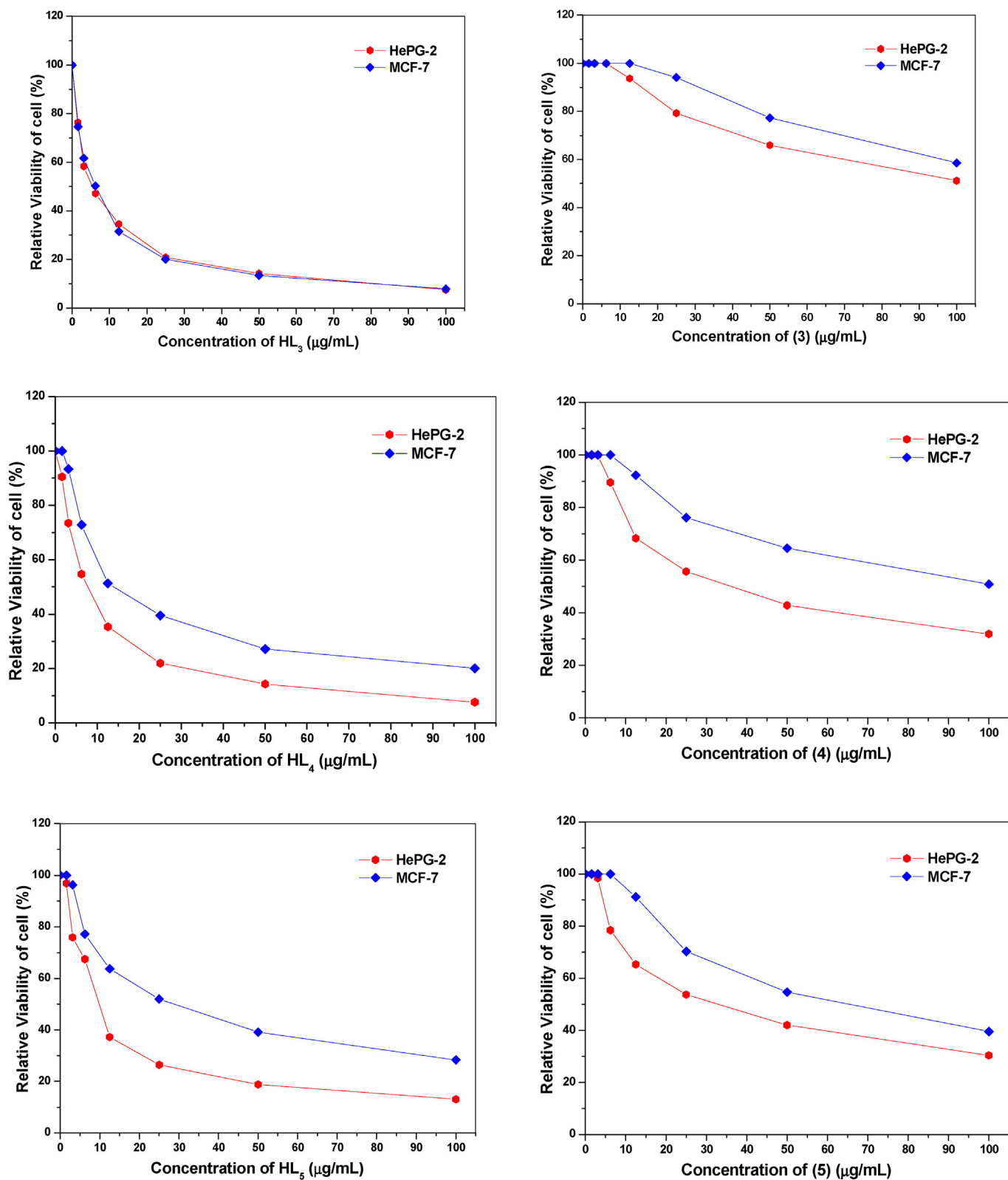


Fig. 16 (continued).

Among all the ligands tested against MCF-7 cell line **HL₃** is exhibiting very good cytotoxic activity, but ligands **HL₁**, **HL₂**, **HL₄** and **HL₅** are exhibiting good to moderate cytotoxic activity as shown in Table 14.

All cobalt(II) complexes are exhibiting moderate to weak cytotoxic or non-cytotoxic activity. Apparently, complexation reduces the cytotoxic activity of ligands. Comparing results with 5-fluorouracil (5-FU)

Table 14

Inhibition of cell viability of ligands (**HL_n**) and their Co(II) complexes (**1–5**) against HePG-2 and MCF-7 cells in comparison with standard drug 5-fluorouracil.

Compound	Cell lines [IC ₅₀ (μg/mL)]	
	HePG-2	MCF-7
5-FU	7.9 ± 0.24	5.6 ± 0.13
HL₁	8.3 ± 0.47	19.4 ± 1.27
HL₂	9.0 ± 0.68	41.5 ± 3.41
HL₃	5.4 ± 0.31	5.6 ± 0.21
HL₄	7.9 ± 0.38	17.6 ± 1.10
HL₅	10.3 ± 0.97	29.5 ± 1.29
(1)	34.8 ± 3.15	81.6 ± 4.87
(2)	12.4 ± 1.04	67.0 ± 4.11
(3)	96.5 ± 6.35	>100
(4)	37.1 ± 2.98	93.5 ± 6.37
(5)	32.9 ± 2.32	62.7 ± 4.12

Data presented as mean ± SD. IC₅₀ (μg/ml): 1–10 (very strong), 11–20 (strong), 21–50 (moderate), 51–100 (weak) and above 100 (non-cytotoxic). All the compounds and the standard dissolved in DMSO, diluted with culture medium containing 0.1% DMSO. The control cells were treated with culture medium containing 0.1% DMSO.

response indicated that **HL₃** have higher cytotoxic activity than 5-FU. The other compounds also showed cytotoxic activity but at higher IC₅₀ values. The results indicated the importance of different heterocyclic rhodanine derivatives in enhancing the cytotoxic activity.

3.12. Antioxidant activity

Oxygen is vital for aerobic life process. However about 5% or more of the inhaled O₂ is converted to reactive oxygen species (ROS). A free radical (FR) can be defined as a chemical species possessing an unpaired electron. FR can be positively charged, negatively charged or electrically neutral [48]. When generation of ROS overtakes the antioxidant defense of the cells, the free radicals start attacking the cell proteins, lipids and carbohydrates which leads to a number of physiological disorders [49]. Free radicals have been implicated in the pathogenesis of diabetes, liver damage, nephrotoxicity, inflammation, cancer, cardiovascular disorders, neurological disorders and in the process of aging [50].

Antioxidants are chemical substances that donate an electron to the free radical and convert it to a harmless molecule. They may reduce the energy of the free radical or suppress radical formation or break chain propagation or repair damage and reconstitute membranes.

Table 15 expressed results of radical scavenging ability and percentage of inhibition of each ligands (**HL_n**), their Co(II) complexes (**1–5**) and standard ascorbic acid, as a reference compound by ABTS method. The results showed that all ligands have high antioxidant activity and have asymptotic effect of ascorbic acid. **HL₃** presented the better activity among all other compounds and when compared with ascorbic acid. There are poor antioxidant activity for Co(II) complexes (**1–5**). The

Table 15

Results of radical scavenging activity and % of inhibition of each ligands (**HL_n**) and their Co(II) complexes (**1–5**) by ABTS method.

Compounds	Absorbance	% inhibition
Control of ABTS	0.520	0
Ascorbic-acid	0.057	89.0
HL₁	0.070	86.5
HL₂	0.082	84.2
HL₃	0.055	89.4
HL₄	0.068	86.9
HL₅	0.079	84.8
(1)	0.332	36.1
(2)	0.296	43.1
(3)	0.424	18.5
(4)	0.339	34.8
(5)	0.283	45.6

Table 16

Antibacterial and antifungal activities data of ligands (**HL_n**) and their Co(II) complexes (**1–5**).

Compound (mg/ml)	<i>E. coli</i>		<i>S. aureus</i>		<i>C. albicans</i>	
	Diameter of inhibition zone (mm)	% activity index	Diameter of inhibition zone (mm)	% activity index	Diameter of inhibition zone (mm)	% activity index
HL₁	9	37.5	14	63.6	17	65.4
HL₂	3	12.5	7	31.8	6	23.1
HL₃	20	83.3	16	72.7	25	96.1
HL₄	14	58.3	17	77.3	21	80.8
HL₅	6	25.0	10	45.4	14	53.8
(1)	–	–	3	13.6	–	–
(2)	–	–	4	18.2	–	–
(3)	–	–	–	–	–	–
(4)	–	–	2	9.1	–	–
(5)	3	12.5	5	22.7	–	–
Ampicillin	24	100	22	100	–	–
Colitrimazole	–	–	–	–	26	100

Co(II) complex of **HL₃** represented a lower antioxidant activity compared to its un-complexed compound. In accordance with the cytotoxicity testing results, the complexation decreases the biological activity of the synthesized compound.

3.13. Antimicrobial activity

The antimicrobial activity of ligands (**HL_n**) and their Co(II) complexes (**1–5**) were tested against bacteria and fungi (yeast) for detecting their antimicrobial activities [9,51,52]. The used organisms in the present investigations included Gram negative (*E. coli*) bacteria, Gram positive (*Staphylococcus aureus*) and yeast (*Candida albicans*). The results of the antibacterial activities of the synthesized compounds are recorded in Table 16. All **HL_n** were found to have antibacterial activity against Gram negative bacteria; namely; *E. coli* (inhibition zone = 9 mm with activity index 37.5% for **HL₁**, inhibition zone = 3 mm with activity index 12.5% for **HL₂**, inhibition zone = 20 mm with activity index 83.3% for **HL₃**, inhibition zone = 14 mm with activity index 58.3% for **HL₄** and inhibition zone = 6 mm with activity index 25% for **HL₅**). Only complex (**5**) has antibacterial activity against Gram negative bacteria; namely; *E. coli* (inhibition zone = 3 mm with activity index 12.5%).

All compounds under investigation have antibacterial activity against Gram positive bacteria; namely *S. aureus* (inhibition zone = 14 mm with activity index 63.6% for **HL₁**, inhibition zone = 7 mm with activity index 31.8% for **HL₂**, inhibition zone = 16 mm with activity index 72.7% for **HL₃**, inhibition zone = 17 mm with activity index 77.3% for **HL₄**, inhibition zone = 10 mm with activity index 45.4% for **HL₅**, inhibition zone = 3 mm with activity index 13.6% for complex (**1**), inhibition zone = 4 mm with activity index 18.2% for complex (**2**), inhibition zone = 2 mm with activity index 9.1% for complex (**4**) and inhibition zone = 5 mm with activity index 22.7% for complex (**5**)) while complex (**3**) has no activity. Only ligands **HL_n** have antifungal activity against *C. albicans* (inhibition zone = 17 mm with activity index 65.4% for **HL₁**, inhibition zone = 6 mm with activity index 23.1% for **HL₂**, inhibition zone = 25 mm with activity index 96.1% for **HL₃**, inhibition zone = 21 mm with activity index 80.8% for **HL₄** and inhibition zone = 14 mm with activity index 53.8% for **HL₅**). **HL_n** were found to have high antibacterial and antifungal activities than their complexes (Fig. 17). **HL₃** was found to have high antibacterial activity against *E. coli* (Fig. 17a) and antifungal activity against *C. albicans* (Fig. 18) more than the other ligands. **HL₄** was found to have high antibacterial activity against *S. aureus* as shown in Fig. 17(b) more than other ligands. **HL₃** and **HL₄** are good antibacterial and antifungal agents.

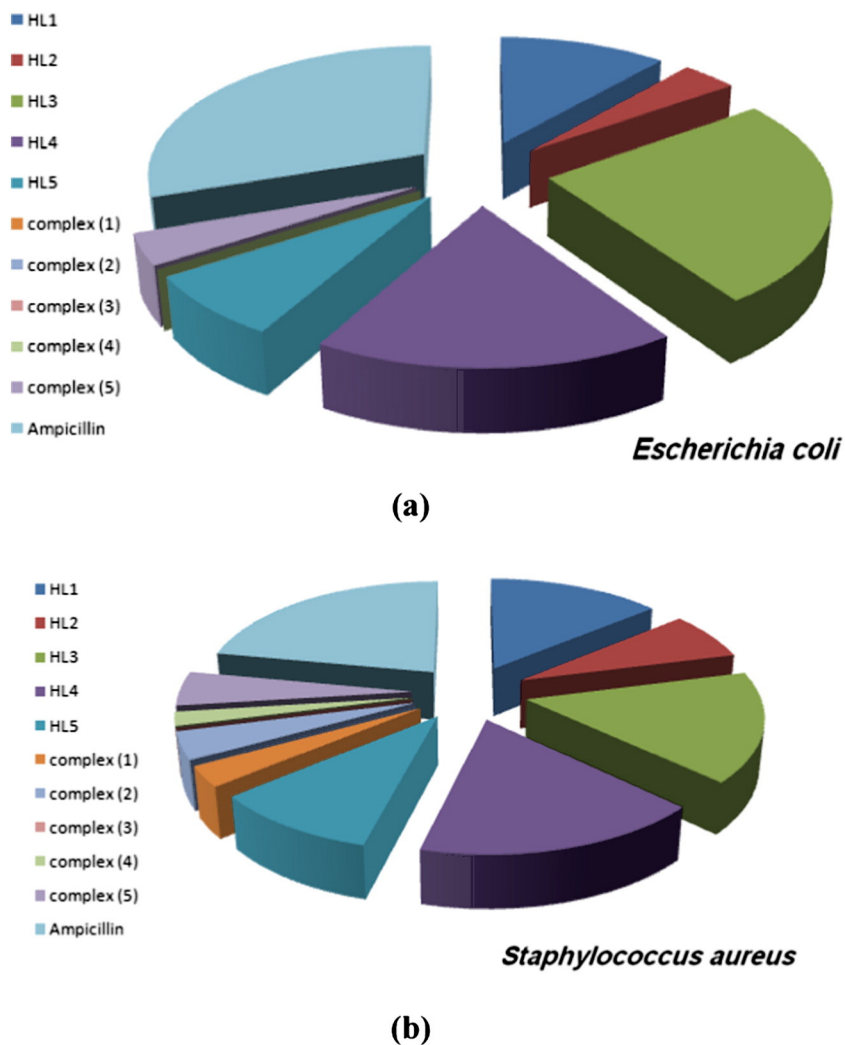


Fig. 17. Antibacterial activity data of ligands (HL_n) and their Co(II) complexes against (a) *Escherichia coli* and (b) *Staphylococcus aureus*.

4. Conclusion

The IR, 1H -NMR spectra show that ligands (HL_n) exist in tautomeric between both states enol/hydrazo form with intramolecular hydrogen bonding. The ligands coordinate to cobalt(II) as monobasic tetradentate. The cobalt(II) complexes are non-electrolytes, paramagnetic and six-coordinated octahedral polymeric complexes of structure $[(Co)_2(L_n)_2(HL_n)(CH_3COO)_2(H_2O)_2]_n$. It is clear that, the four

bonding sites are 3-NH, CS, CO and hydrazo groups. The XRD patterns of ligands indicate that the powder is a mixture of amorphous and polycrystals nature. The polymeric complexes exhibit amorphous nature. The interaction between ligands (HL_n) and SS-DNA involves a hypochromism effect coupled with bathochromism. There are straight line relationships between energy gap (ΔE) and the SS-DNA binding activity (K_b) of the ligands with Hammett's p -substitution coefficients (σ^R). It is clear that that the values of energy gap (ΔE) and the SS-

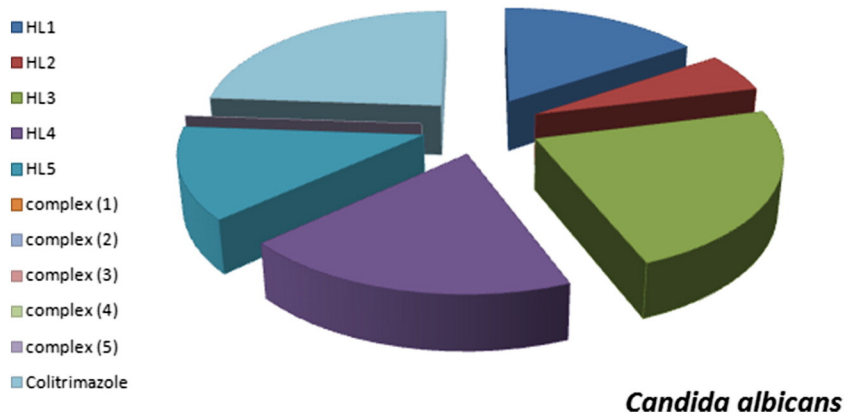


Fig. 18. Antifungal activity data of ligands (HL_n) and their Co(II) complexes against *Candida albicans*.

DNA binding activity (K_b) increase with increasing α^R . Rhodanine derivatives have been evaluated to have biological and pharmacological activities. **HL₃** has the highest cytotoxic, antioxidant and antimicrobial activities.

References

- [1] A.Z. El-Sonbati, M.A. Diab, A.A. El-Bindary, Sh.M. Morgan, *Inorg. Chim. Acta* 404 (2013) 175–187.
- [2] A.Z. El-Sonbati, M.A. Diab, A.A. El-Bindary, Sh.M. Morgan, *Spectrochim. Acta A* 127 (2014) 310–328.
- [3] N.A. El-Ghamaz, A.Z. El-Sonbati, M.A. Diab, A.A. El-Bindary, M.K. Awad, Sh.M. Morgan, *Mater. Sci. Semicond. Process.* 19 (2014) 150–162.
- [4] A.Z. El-Sonbati, A.F. Shoair, A.A. El-Bindary, M.A. Diab, A.S. Mohamed, *J. Mol. Liq.* 209 (2015) 635–647.
- [5] A.Z. El-Sonbati, A.A.M. Belal, M.S. El-Gharib, Sh.M. Morgan, *Spectrochim. Acta A* 95 (2012) 627–636.
- [6] A.Z. El-Sonbati, M.A. Diab, A.A.M. Belal, Sh.M. Morgan, *Spectrochim. Acta A* 99 (2012) 353–360.
- [7] A.A. Al-Sarawy, A.A. El-Bindary, D.N. El-Sonbati, *Spectrochim. Acta A* 61 (2005) 1847–1851.
- [8] N.A. El-Ghamaz, A.Z. El-Sonbati, Sh.M. Morgan, *J. Mol. Struct.* 1027 (2012) 92–98.
- [9] M.I. Abou-Dobara, A.Z. El-Sonbati, Sh.M. Morgan, *World J. Microbiol. Biotechnol.* 29 (2013) 119–126.
- [10] A.Z. El-Sonbati, M.A. Diab, A.A. El-Bindary, G.G. Mohamed, Sh.M. Morgan, *Inorg. Chim. Acta* 430 (2015) 96–107.
- [11] M.A. Diab, A.Z. El-Sonbati, A.A. El-Bindary, G.G. Mohamed, Sh.M. Morgan, *Res. Chem. Intermed.* 41 (2015) 9029–9066.
- [12] X.H. Zhang, L.Y. Wang, Z.X. Nan, S.H. Tan, Z.X. Zhang, *Dyes Pigments* 79 (2008) 205–209.
- [13] K.L. Reddy, K.R.Y. Harish, K.K. Ashwini, S.S.S. Vidhisha, *Nucleosides Nucleotides Nucleic Acids* 28 (2009) 204–219.
- [14] A.A. El-Bindary, A.Z. El-Sonbati, R.M. Ahmed, *Spectrochim. Acta A* 58 (2002) 333–339.
- [15] M. Maghami, F. Farzaneh, J. Simpson, M. Ghiasi, M. Azarkish, *J. Mol. Struct.* 1093 (2015) 24–32.
- [16] R.C. Maurya, B.A. Malik, J.M. Mir, P.K. Vishwakarma, D.K. Rajak, N. Jain, *J. Mol. Struct.* 5 (2015) 266–285.
- [17] Z. Wang, L. Tang, Y. Zhang, S. Zhan, J. Ye, J. Power, *Sources* 287 (2015) 50–57.
- [18] A.Z. El-Sonbati, M.A. Diab, A.A. El-Bindary, A.M. Eldesoky, Sh.M. Morgan, *Spectrochim. Acta A* 135 (2015) 774–791.
- [19] N.A. El-Ghamaz, M.A. Diab, A.A. El-Bindary, A.Z. El-Sonbati, H.A. Seyam, *J. Mater. Sci. Semicond. Proc.* 27 (2014) 521–531.
- [20] M. Sirajuddin, S. Ali, N.A. Shah, M.R. Khan, M.N. Tahir, *Spectrochim. Acta A* 94 (2012) 134–142.
- [21] S. Dey, S. Sarkar, H. Paul, E. Zangrando, P. Chattopadhyay, *Polyhedron* 29 (2010) 1583–1587.
- [22] M. Sirajuddin, S. Ali, *Synthesis and Characterization of Potential Bioactive Organotin*, LAP, Germany, 2013.
- [23] A. Wolfe, G.H. Shimer, T. Meehan, *Biochemistry* 26 (1987) 6392–6396.
- [24] T. Mosmann, *J. Immunol. Methods* 65 (1983) 55–63.
- [25] F. Denizot, R. Lang, *J. Immunol. Methods* 22 (1986) 271–277.
- [26] E. Lissi, B. Modak, R. Torres, J. Escobar, A. Urza, *Free Radic. Res.* 30 (1999) 471–477.
- [27] A.B.A. El-Gazar, A.M.S. Youssef, M.M. Youssef, A.A. Abu-Hashem, F.A. Badria, *Eur. J. Med. Chem.* 44 (2009) 609–624.
- [28] R. Aeschlach, J. Loliger, C.B. Scott, A. Murcia, J. Butler, B. Halliwell, I.O. Aruoma, *Food Chem. Toxicol.* 32 (1994) 31–36.
- [29] A.F. Shoair, *J. Coord. Chem.* 60 (2007) 1101–1109.
- [30] A.Z. El-Sonbati, M.A. Diab, M.M. El-Halawany, N.E. Salem, *Spectrochim. Acta A* 77 (2010) 735–766.
- [31] G.J. Karabatores, B.L. Shapiro, E.M. Vane, J.S. Fleining, J. Ratka, *J. Am. Chem. Soc.* 85 (1963) 2784–2788.
- [32] A.Z. El-Sonbati, A.A. El-Bindary, A. El-Dissouky, T.M. El-Gogary, A.S. Hilali, *Spectrochim. Acta A* 58 (2002) 1623–1629.
- [33] S. Sen, S. Shit, S. Mitra, S.R. Battren, *J. Struct. Chem.* 19 (2008) 137–142.
- [34] A.Z. El-Sonbati, A.A. El-Bindary, E.M. Mabrouk, R.M. Ahmed, *Spectrochim. Acta A* 57 (2001) 1751–1757.
- [35] K. Nakamoto, *Infrared and Raman Spectra of Inorganic and Coordination Compounds*, Wiley Interscience Publication John Wiley & Sons, Inc., New York, 1986.
- [36] K. Nakamoto, *Infrared Spectra of Inorganic and Coordination Compounds*, John Wiley, New York, 1986.
- [37] U. Ryde, *Biophys. J.* 77 (1999) 2777–2787.
- [38] W.H. Mahmoud, N.F. Mahmoud, G.G. Mohamed, A.Z. El-Sonbati, A.A. El-Bindary, *Spectrochim. Acta A* 150 (2015) 451–460.
- [39] K. Dakshayani, Y. Lingappa, M.S. Kumar, S. Rao, *J. Chem. Pharm. Res.* 3 (2011) 506–513.
- [40] F.C. Brown, C.K. Bradsher, B.F. Moser, S. Forrester, *J. Organomet. Chem.* 24 (1959) 1056–1060.
- [41] A.W. Coats, J.P. Redfern, *Nat. J.* 20 (1964) 68–79.
- [42] H.W. Horowitz, G. Metzger, *J. Anal. Chem.* 35 (1963) 1464–1468.
- [43] E.C. Long, J.K. Barton, *J. Chem. Res.* 23 (1990) 271–273.
- [44] Q. Wang, X. Wang, Z. Yu, X. Yuan, K. Jiao, *Int. J. Electrochem. Sci.* 6 (2011) 5470–5481.
- [45] M. Sirajuddin, S. Ali, A. Badshah, *J. Photochem. Photobiol. B Biol.* 124 (2013) 1–19.
- [46] M. Tariq, N. Muhammad, M. Sirajuddin, S. Ali, N.A. Shah, M.R. Khan, M.N. Tahir, *J. Organomet. Chem.* 723 (2013) 79–89.
- [47] J.P. Costes, F. Dahan, J.P. Laurent, M. Drillon, *Inorg. Chem. Acta* 294 (1999) 8–12.
- [48] K.H. Cheseman, T.F. Slater, *Br. Med. Bull.* 49 (1993) 481–493.
- [49] R.S. Cotran, V. Kumar, T. Collins, *Robbin's Pathological Basis of Diseases*, sixth ed. Thomson Press (I) Ltd., Noida and India, 1999.
- [50] S.K. Mondal, G. Chakraborty, M. Gupta, U.K. Mazumdar, *Indian J. Exp. Biol.* 44 (2006) 39–44.
- [51] N.H. Metwally, M.A. Abdalla, M.A.N. Mosselhi, E.A. El-Desoky, *Carbohydr. Res.* 345 (2010) 1135–1141.
- [52] Z.H. Chen, C.J. Zheng, L.P. Sun, H.R. Piao, *Eur. J. Med. Chem.* 45 (2010) 5739–5743.